STRENGTH AND DAMAGE PROGNOSIS OF ADHESIVE BOND AND INTER-PLY HYBRID COMPOSITES BASED ON DIELECTRIC PROPERTIES

by

PRIYANSHU KUMAR BANERJEE

Presented to the Faculty of the Graduate School of

The University of Texas at Arlington in Partial Fulfillment

of the Requirements

for the Degree of

MASTER OF SCIENCE IN MECHANICAL ENGINEERING

THE UNIVERSITY OF TEXAS AT ARLINGTON

December 2017

Acknowledgements

First of all, I would like to express my earnest gratitude to Dr. Kenneth Reifsnider for his continued guidance throughout my research endeavors. I'm forever inspired by his drive to learn something new every day and his vast knowledge in the field of advanced materials. Furthermore, I'd also like to thank Dr. Rassel Raihan for his constant support and motivation. The concepts of Broadband Dielectric Spectroscopy and adhesive bonding were meticulously explained and made clear by him.

Next, I'd like to thank Dr. Ashfaq Adnan for being a part of my thesis defense committee.

I'd also like to acknowledge my sincere thanks to Ron LaPosa and Dave Manivanh from the University of Texas at Arlington Research Institute for training me on all the lab equipment. Finally, this research would not have been possible without the unending encouragement and assistance from my colleagues – Muthu Ram Prabhu Elenchezhian and Vamsee Vadlamudi.

Abstract

STRENGTH AND DAMAGE PROGNOSIS OF ADHESIVE BOND AND INTER-PLY HYBRID COMPOSITES BASED ON DIELECTRIC PROPERTIES

Priyanshu Kumar Banerjee, MS

The University of Texas at Arlington, 2017

Supervising Professor: Dr. Kenneth Reifsnider

Composite materials have found their applications in a wide range of industries particularly in the aerospace and automotive sectors. This is because they are comparatively light-weight and provide a much better corrosion and wear resistance as compared to other ceramics and metals. Adhesive bonding can be used to improve the stress distribution between these composite materials. Moreover, adhesive bond decreases the weight and concentration of stresses in the structure.

Broadband Dielectric Spectroscopy, BbDS is a robust tool used for analyzing the dielectric properties of a polymer composite. This method can be used to monitor the curing process of the specimen. Alterations in the material systems result in changes in the dielectric spectra of the heterogeneous materials. With increasing service life, the quality of bond decreases thus resulting in interfacial polarization.

The objective of this study was to establish BbDS as an NDE method to detect the defect in an adhesive bond. In this case, BbDS is employed to measure the changing dielectric properties throughout the length of the specimen. Thus, two different bonded specimen types with varying bond surface quality were made using compression molding – button and single-lap joints. The single-lap joint specimens were then tested for their failure load and a correlation was formulated between the dielectric and mechanical properties. The experimental results were further validated by 2D Finite Element Modeling.

In addition to the above research, a brief study was done on inter-ply hybrid composite specimens. In this case, a similar approach was followed wherein, BbDS was used to measure the dielectric properties of two different types of hybrid composite specimens – unidirectional fabric and woven fabric. These specimens were also tested for their load to failure and a correlation was developed between the dielectric and mechanical characteristics.

Table of Contents

Table of Figures

List of Tables

Dedicated to my Mom and Dad.

Chapter 1

INTRODUCTION

1.1 Adhesive Bonding in Composites

In recent years, there has been a widespread growth in the use of composite materials in the aerospace industry, automobile, energy storage and naval applications. This is because they are comparatively lightweight, have better thermal stability as well as an increased impact resistance as compared to metals. Adhesive can be defined as any polymeric substance that has the capability to hold materials together. The earliest known use of adhesive dates to 36000 years when two stones were attached to a handle by bitumen [17]. However, the Industrial Revolution proved to be a quantum leap towards the development of materials used in the composition of new adhesives. Adhesive bonding is one of the many methods used for joining materials. The other methods are soldering, crimping, welding, brazing with the most popular being mechanical fastening. The stress distribution can be vastly reduced in a composite Nowadays, almost 50% of the airframe in a military aircraft is made of adhesive bonded CFRP. The figure shows a Swedish military aircraft JAS Gripen, in which different composite parts have been bonded using an adhesive as shown below

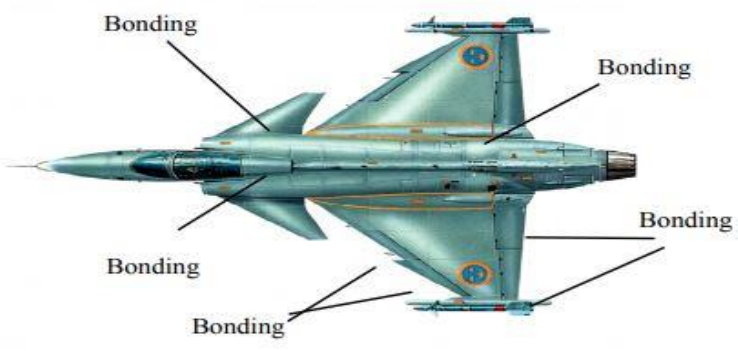

Figure 1-1: Swedish Military Aircraft JAS Gripen [17]

However, there are various parameters that can affect the performance of an adhesive bond. They are as given below:

1. Quality of the adherend surface.
2. Materials to be joined.
3. Magnitude and direction of the loads resisted by the joint.
4. Temperature, humidity or the surroundings in which the bond is made.
5. Bond durability
6. Cure time, the quantity of adhesive used, number of coats applied etc.

A change in any one of the above parameters can cause serious discrepancies in the strength and quality of the bond. This will ultimately lead to bond failure. There are three primary modes of failure as given below [2]:

1. Adhesive failure: This occurs when the bonded joint fails between the adhesive and the adherend surface.
2. Cohesive failure: This result when the adhesive joint fails within the adhesive layer.
3. Adherend failure: This type of failure occurs when the composite structure fails in between the layers as shown below.

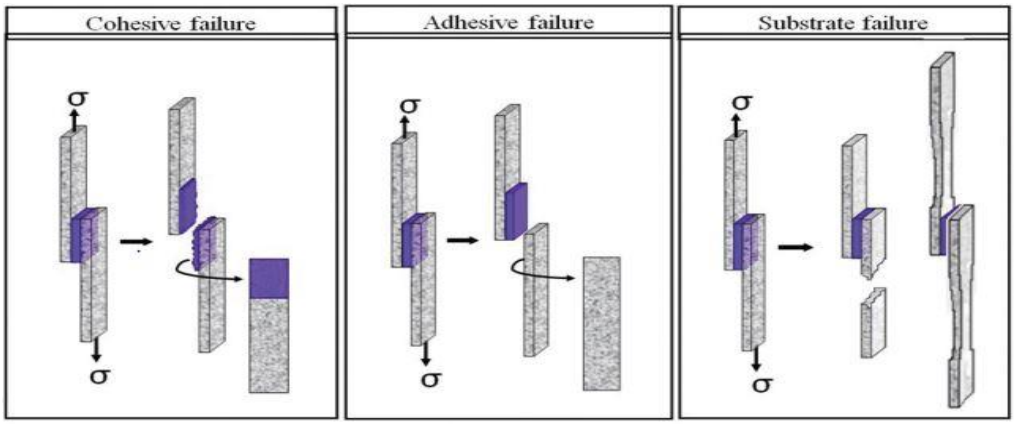

Figure 1-2: Types of adhesive bond failure [23]

A multitude of NDE methods is available that can detect many different problems in an adhesive joint. Some of them are listed in the table below [18].

Table 1-1: Types of NDE methods available [18]

Technique	**Potential for inspection of adhesive joints**
X-ray	Some
Shearography	Detection of disbonds
Thermography	As above
Holography	As above
Ultrasonics	Excellent, the most commonly used
Microwave	Poor
Visual	Poor
Radar	Poor
Dye Penetrant	None
MRI	Detection of state of cure and possibly presence of moisture
Eddy Current	Poor
Dielectric	Detection of state of cure and possibly presence of moisture
Neutron Radiography	Properties/presence of adhesive
Mechanical Impedance	Poor
IR Spectroscopy	Moisture detection

Heterogeneous composite materials are universally dielectric material systems. The dielectric properties of these material systems are affected by numerous parameters such as heterogeneity of morphological and electrical properties of the constituent phases, intra-particle structure, particle size, shape morphology and orientation as well as the

structural and electrical interactions between particles. Thus, a series of material state and morphological changes occur with growing decay. To obtain the material information and morphological changes caused due to multiple defect occurrences, Broadband Dielectric Spectroscopy was adopted. What makes a heterogeneous composite material stand out is its ability to regulate the shape, size, properties, and interface of the system thus allowing it to get by with its environment. As the service life of system increases, the material states go through a lot of changes. Also, a lot of factors are taken into account while predicting the damage tolerance, fracture toughness and structural integrity of the material. These include the defect growth relationships, appropriate balance equations and constitutive equations with differing material properties. Other than that, the local changes may also lead to substantial effects in predicting the performance of the composite systems.

1.2 Motivation and Background

There are very few Non-Destructive Testing methods available to detect a weak adhesion bond or 'kissing bond' in an adhesive joint. This occurs when the adherend surfaces are in close contact with each other with limited bonding between them. Broadband Dielectric Spectroscopy is already being used as a leading mechanism for analyzing the dielectric behavior in a material. The objective of my research is to use Broadband Dielectric Spectroscopy (BbDS) as a characterization tool to predict the location of the defect in an adhesive bond. Besides that, I've also tried to broaden my research by including hybrid composites and its dielectric behavior in that matter using Broadband Dielectric Spectroscopy.

Chapter 2

LITERATURE REVIEW

2.1 Kissing Bond

The use of adhesive bonding in the aerospace industry has not been up to the mark. This is because there are not many NDT methods available to trace the weak adhesion bond i.e. kissing bond. The actual nature of a kissing bond was studied by artificially manufacturing a defective metal-metal adhesive bond. The bonding procedure satisfied the metal-to-metal bonding standards and the kissing bond requirements. Thus, a criterion was developed which differentiates kissing bond from a regular defective bond. They are as follows [10]:

1. The strength of the bond determined after a lap shear test should be less than 20% of the actual strength.
2. The mode of failure should be an adhesive failure as opposed to cohesive or adherend failure.
3. While performing a traditional Ultrasonic C-scan mapping, a kissing bond should remain indistinguishable from a normal bond.

There are three primary defects that can take place in an adhesive bond. Voids in an adhesive layer, complete disbonds and poor cohesion occurring in a weak adhesive layer or weak adhesion which results due to a weak interface between the adhesive layer and one or both the adherend surfaces. A considerable amount of progress has been made in the detection of voids, porosity and disbonds. However, the same cannot be said for poor adhesion or cohesion in that matter [9].

The three main reasons for adhesive failure are mentioned below [6]:

1. The adherend surface is susceptible to deterioration during the manufacturing phase. This, in turn, gives rise to a chemically unstable surface.
2. Sub-standard surface preparation procedure.
3. The curing of the adhesive occurs prior to bond formation.

A kissing bond, also known as a weak adhesion bond arises due to a plastic contact between two rough surfaces. The cohesive properties remain unaltered in this type of defect. Ultrasonic inspection has been the most researched nondestructive evaluation (NDE) method for the detection of a kissing bond. A high-frequency normal incidence transducer was used to detect kissing bond which usually remains undetected by traditional ultrasonic bond testers. The transducer is directed below the surface of the adherend to generate two focal zones using highly focused transducers- one for longitudinal waves and other for transverse waves. Finally, the weak bond was detected using transverse vibrations since it resulted in better acoustic disparity as compared to the longitudinal ones [7].

There are various methods by which one can artificially create defects inside a material. Flat bottom holes, inserts and ‘real’ damage being the most common of them all. They are as shown below [19].

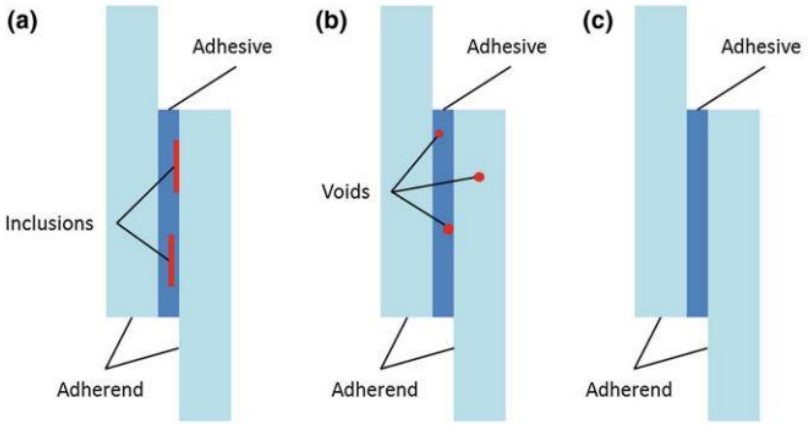

Figure 2-1: Types of defects observed in adhesive joints; a) inclusions, b) voids and c) kissing defects [19]

A kissing bond defect, on the contrary, can be simulated in two ways- dry contact and liquid layer. When an adhesive layer is cured after being applied to one of the adherend surfaces and followed by compressing it on the other surface, it's called a dry contact defect. A liquid layer defect, on the other hand, is produced by incorporating an external impurity between the adhesive layer and the adherend surface. In both cases, the adhesive and the adherend surface are not in any physical contact at the location of the defect [1].

To achieve a higher durability for the adhesive bond, suggested the following steps as given below [6].

1. Degrease the adherend surface completely by proper surface preparation methods.
2. Clear away the chemically inert topmost layer from the adherend surface prior to bonding
3. This will give rise to a surface which will be immune to hydration occurring between the adhesive bonds.

2.2 Broadband Dielectric Spectroscopy

Broadband Dielectric Spectroscopy (BbDS) is the study of the interaction of electromagnetic waves with the matter at different frequency ranges ranging from 10^{-6} Hz to 10^{12} Hz. Thus, one can study the molecular and combined dipolar fluctuations, the transport of charge developing inside the boundaries of materials and effects of polarization. The effect of the various polarization techniques on the dielectric response is shown in the figure below [5].

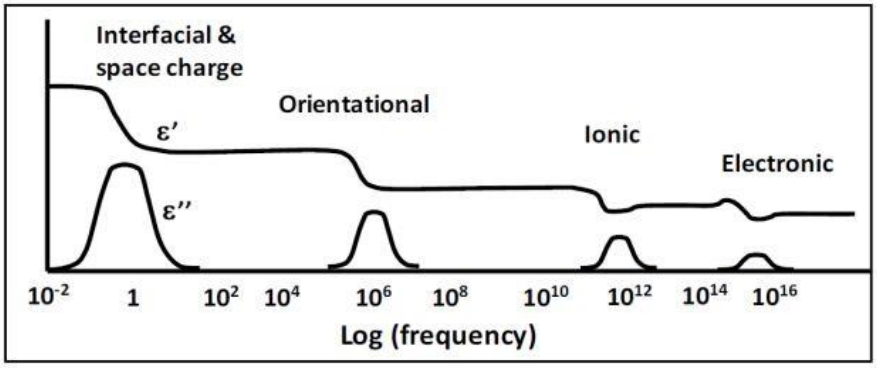

Figure 2-2: Dielectric response of material constituents with varying broadband frequency range [5]

The difference between the electrical properties results in polarization inside a heterogeneous material. This phenomenon was observed by Maxwell in the equations given below:

$$\nabla \cdot \vec{D} = \rho \tag{1}$$

$$\nabla \times \vec{H} = \vec{j} + \frac{\partial \vec{D}}{\partial x} \tag{2}$$

$$\nabla \times \vec{E} + \frac{\partial \vec{B}}{\partial x} = 0 \tag{3}$$

$$\nabla \cdot \vec{B} = 0 \tag{4}$$

In the above equations, $\vec{D}$ is the dielectric displacement, $\vec{H}$ is the magnetic field, ρ being the charge density, $\vec{j}$ is the ohmic current density and $\vec{B}$ the magnetic induction. Th electric field must satisfy the continuity equations as given below:

$$\nabla \cdot \vec{j} + \frac{\partial \vec{\rho}}{\partial t} = 0 \tag{5}$$

For linear materials, the dielectric displacement $\vec{D}$ and electric field $\vec{E}$ can be correlated as follows

$$\vec{D} = \varepsilon_0 \vec{E} + \vec{P} \tag{6}$$

Similarly, polarization and charge density in the absence of external source is given as

$$\nabla \cdot \vec{P} = -\rho \tag{7}$$

Also, the dielectric displacement $\vec{D}$ is directly proportional to the electric field $\vec{E}$ where the proportionality constant is ε as shown below

$$D = \varepsilon \varepsilon_0 \vec{E} \tag{8}$$

In the above equation, the dielectric nature of the material is characterized by ε, also known as the relative permittivity of the material. From (6) and (8), we can derive polarization as follows

$$P = \varepsilon_0 \chi E \equiv \varepsilon_0 (\varepsilon - 1)\vec{E} \tag{9}$$

In this case, χ is the polarization co-efficient also known as dielectric susceptibility [29].

There are various polarizations mechanisms that occur in a material system at different frequency ranges as shown in the figure below.

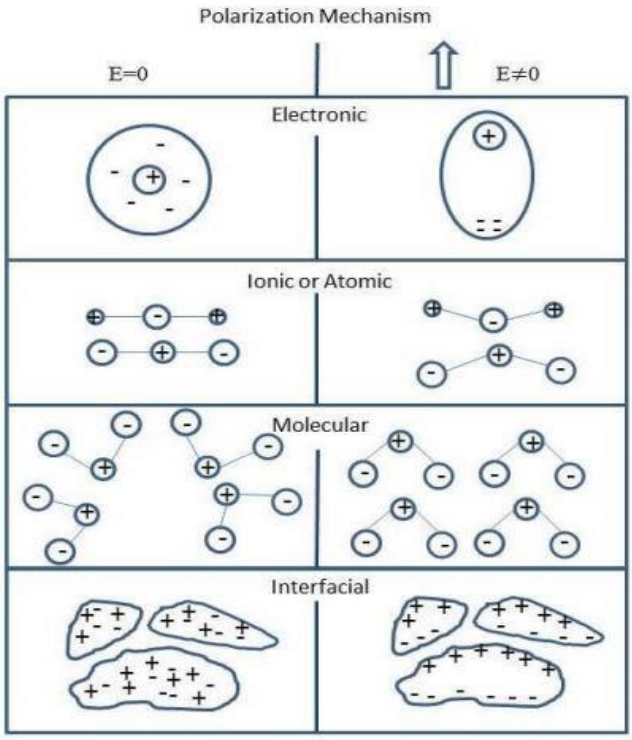

Figure 2-3: Different polarization mechanisms occurring in a material [14]

Since heterogeneous materials are naturally dielectric, any change in the morphology or interaction of permittivity will affect the polarizations and complex electric fields. Using experimental validation, Baker et al established that polarization, on a local level, is greatly influenced by the product of electric displacement and the potential gradient (electric field). Thus, he concluded that a heterogeneous material interface stores electrical charge [3].

An in-situ setup was developed to measure the dielectric behavior while at the same time inducing the specimen to a mechanical load with increasing micro-crack density. The figure below shows an in-situ response of the dielectric property in different zones of damage progression of a composite coupon sample subjected to monotonic loading. So, any change in the size, shape and orientation of microdamage, volume of the defect and the interface formed was easily identifiable by this method. Thus, it was deduced that study of the dielectric behavior can give us critical information about the change in material state as it undergoes mechanical loading [16].

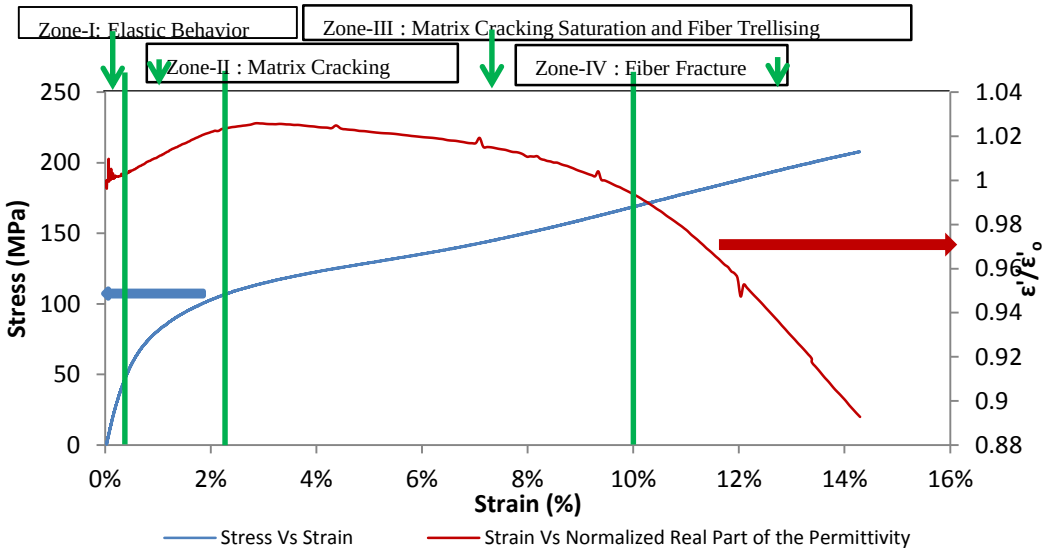

Figure 2-4: Dielectric response in different zones of damage progression [16]

An inverse relationship between break strain and the initial value of the real part of the complex dielectric permittivity of the material was formulated by Raihan et al. Through the thickness values of real and imaginary parts of the dielectric permittivity were measured for 50 coupon specimens. The specimens manufactured using continuous fiber reinforced, glass/epoxy plain weave materials were analyzed over a wide frequency range. The figure below shows the relationship between the mechanical and dielectric properties of the 50

specimens [14].

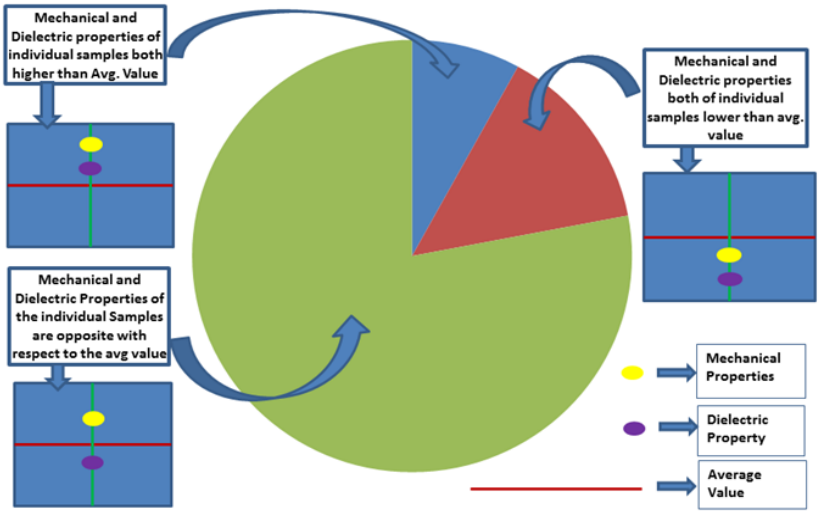

Figure 2-5: Relationship between dielectric and mechanical properties [14]

A comparative study was done and the relative values for each specimen to their subsequent break strength and fracture strain were compared in quasi-static loading

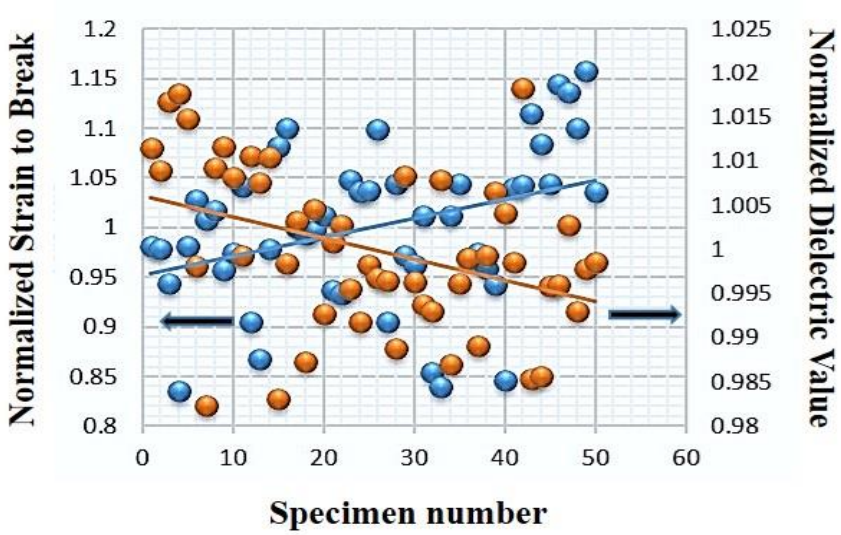

Figure 2-6: Strain to break and corresponding values of initial dielectric real part of the permittivity, as vertical pairs and lines (blue and orange) showing that there is an inverse relationship between these two quantities, with very high significance (Normalization was done by the average breaking strain and average dielectric permittivity) [15]

conditions. Thus, it was proved that higher interfacial polarization is a result of high dielectric permittivity which on the other is related to lower breaking strain of the specimen as shown in the figure above [15].

A similar technique, Electrochemical Impedance Spectroscopy (EIS) was employed by Fazzino et al to distinguish damage in a composite material. This was done by examining the impedance values of pre-fatigued glass fiber specimens soaked in NaCl solution for a day. The setup for EIS is shown in the figure below.

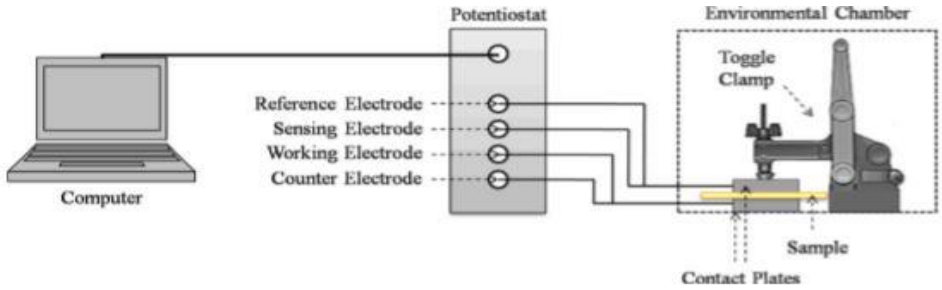

Figure 2-7: Electrochemical Impedance Spectroscopy experimental setup for checking damage [8]

Based on the results obtained from this method, it was proposed that the internal micro-structure of a specimen varies as the damage grows. These micro-cracking locations emerged as sites for moisture build-up due to their hydrophilic nature. Thus, the impedance

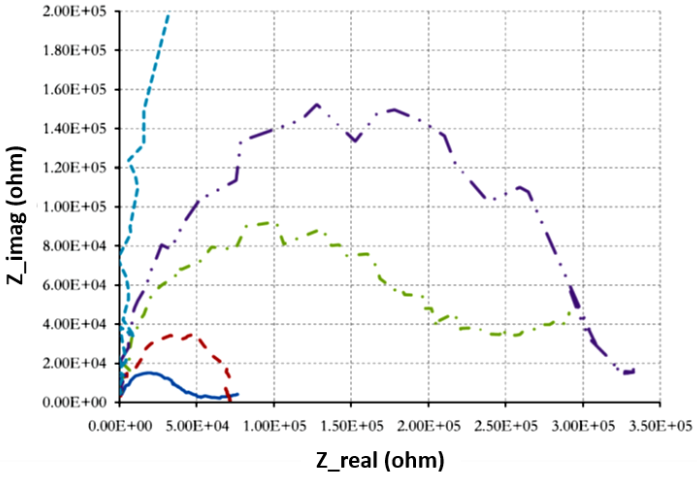

Figure 2-8: Nyquist Plot – 90^{o} specimen [8]

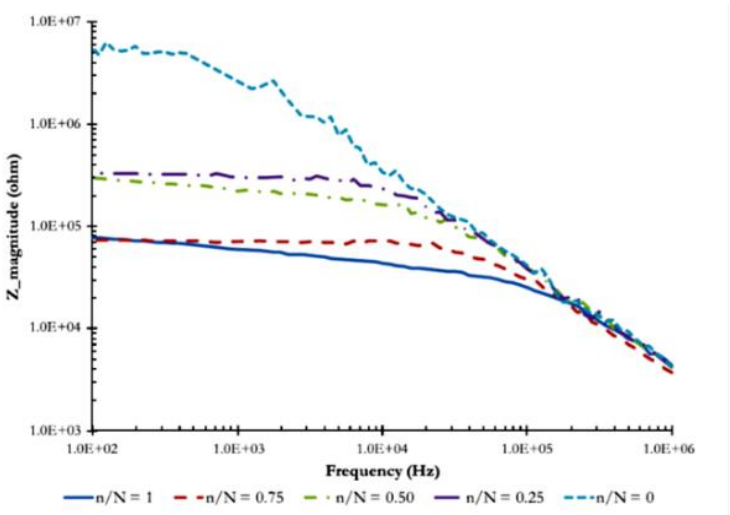

Figure 2-9: Bode Plot – 90^{o} specimen [8]

values were plotted for three different fiber orientations (0^{o},45^{o},90^{o}) at four different fatigue levels (0,0.25,0.50 and 0.75). The imaginary versus the real impedance graph was plotted in a Nyquist plot while Bode plot was used to plot the magnitude of impedance versus frequency for a 90^{o} specimen as shown in the figures below [8].

The BbDS technique was also used to measure the frequency domain response of single-lap joint specimens by securing the effect of defects at the adhesive bond interface. Thus, helping in differentiating the different material states of kissing bond. The dielectric data obtained using this method was then used to predict the presence of interfacial defects while also detecting changes if any of the mechanical properties [11],

2.3 Dielectric relaxation

The complex permittivity ε* derived from Maxwell's equations is a time or frequency dependent property that occurs when time-dependent processes develop within the specimen. The molecular fluctuation of dipoles, due to their motion in a potential field results in the dielectric relaxation phenomena. Due to the motion of mobile charge carriers (ions, electrons and charged defects), the dielectric response turns out to be conductive.

Thus, time-dependent processes are responsible for variations in the applied electrical field E(t) and resulting dielectric displacement D(t) [5].

However, the relaxation phenomenon is basically due to the following:

1. Microscopic fluctuations of molecular dipoles
2. Propagation of mobile charge carriers by translational diffusion of electrons, holes or ions.
3. The separation of charges at interfaces which gives rise to an additional polarization. The latter can take place at inner dielectric boundary layers on a mesoscopic scale and/or at the external electrodes contacting the sample (electrode polarization) on a macroscopic scale.

Relaxation processes are represented by some common features with increasing frequency as given in the complex dielectric function below.

$$\varepsilon^* = \varepsilon'(\omega) - i\,\varepsilon''(\omega) \tag{10}$$

In the above equation, the real part of the dielectric function $\varepsilon'(\omega)$ decreases with increasing frequency whereas the imaginary part $\varepsilon''(\omega)$ is represented by a peak as shown in the figure below. It shows an increase in the imaginary part of the dielectric function which indicates the conduction phenomena. The real part, on the other hand, is independent of frequency for purely ohmic conduction and increases with decreasing frequency for ionic conduction [5].

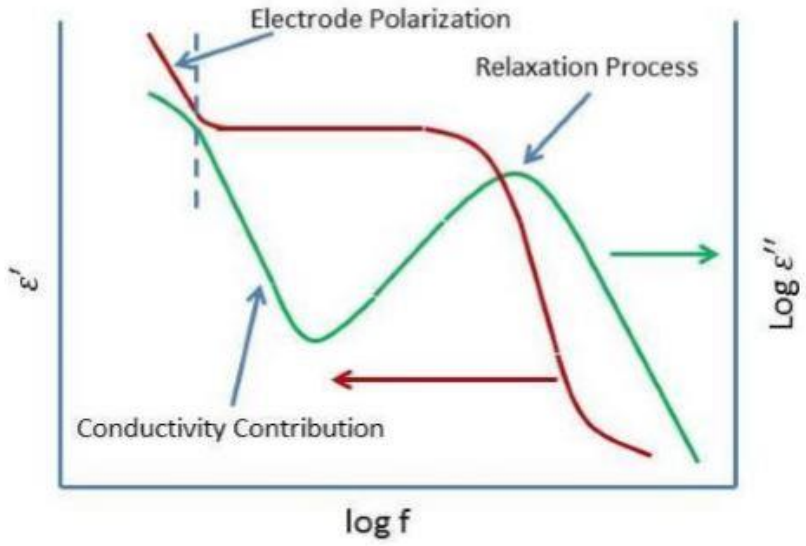

Figure 2-10: Real permittivity $\varepsilon'(\omega)$ (solid line) and imaginary permittivity $\varepsilon"(\omega)$ of the complex dielectric function occurring during relaxation of an ionic conductive material [5]

The complex conductivity σ^* and the complex electric modulus M^* are some of the other parameters that can be used to denote the dielectric behavior of materials. It can be used to depict the transport of charge and various forms of polarization at different frequency ranges [4] [5].

Heterogeneous composite materials are good dielectrics which means that they can store charge at their interface, defects, micro-cracks and micro-boundaries. Although being poor conductors, they have quite a few conduction mechanisms. Since they develop many micro-interfaces, as decay occurs it gives rise to new 'phases' in the system. Thus, the nature of contact changes when materials with varying electrical properties come in contact with each other resulting in further decay. The charge build-up on the interface results in interfacial polarization which leads to dielectric relaxation. The electrical properties and details about the heterogeneous structure of the material is given by its dielectric relaxation. The number of interfaces, shape and orientation of inclusions relative to the vector direction all plays an important role in the extent of dielectric relaxations

expected in a heterogeneous system. Nevertheless, most of the dielectric relaxations anticipated are not actually observed due to sensitivity in the evaluation and an inadequate frequency range [14].

Chapter 3

EXPERIMENTAL FACILITIES

The process starts with manufacturing the carbon-fiber reinforced laminate using compression molding in a Wabash Vantage series hydraulic press. The manufactured laminates were then cut using a tile sawyer into two different types of specimens with varying geometries. The surface of these specimens was sanded prior to bonding them using an aerospace grade adhesive. This was followed by analyzing the dielectric properties using the Novocontrol Broadband Dielectric/Impedance Spectrometer. Finally, an MTS Landmark™ system was used to perform axial monotonic tests to predict the strength of the bonded specimens.

3.1 Compression Molding

The Wabash Vantage Series Hydraulic Press was used to manufacture the composite specimens.

Figure 3-1: Wabash Vantage Series Hydraulic Press for compression molding

The compression molding process is divided into three parts tooling, layup and curing.

1. Tooling: In this step, a flat and smooth aluminum plate, approx. 0.25 to 0.50-inch thick was used as a mold for laying up the raw material prepreg. Prior to the layup, the mold is cleaned with an acetone solvent or similar.
2. Layup: The raw material prepreg used in this case was Torayca T700S/G94 plain weave carbon fiber prepreg supplied by Rockwest Composites. The prepreg roll was maintained at below $0^{o}F$ prior to being extracted from the freezer for manufacturing. The prepreg was then cut into 4 plies of 10”x10” and placed on the aluminum mold while wrapped in a vacuum bagging film with peel ply in between.
3. Curing: This is the final step in the manufacturing process of the composite laminate. After the plies are laid up, a release film is placed on the top and bottom of the pre-cured four-ply laminate. A release fabric, also known as peel ply is planted between the release film and the 4-ply laminate thus achieving a smooth surface for the specimen.

The next step in the manufacturing process was to cure the 4-ply laminate in the hydraulic press based on the cure cycle provided by the vendors.

3.2 Broadband Dielectric Measurement

3.2.1 Novocontrol™ System

Figure 3-2: Novocontrol Broadband Dielectric/Impedance Spectrometer experimental setup [24]

The Broadband Dielectric/Impedance Spectrometer consists of a Novotherm-HT high-temperature control system with temperatures ranging from ambient to 1200˚C with 0.1˚C resolution. The system includes a Novotherm-HT temperature controller, a furnace and a ceramic sample cell with a movable holder for the Probostat and an Alpha analyzer for impedance analysis. The requirements for this system is given below [24].

Frequency: 3μHz-20MHz

Phase accuracy: 0.002˚ or tan(δ) accuracy $3X10^{-5}$

Impedance range: $10^{-3}\Omega$-$10^{15}\Omega$

Novotherm- HT: Ambient to 1200˚C

3.2.2 Alpha analyzer

The alpha analyzer is used to compute the complex dielectric function, conductivity and impedance properties of the heterogeneous composite material specimens as a function of frequency. Not only can it measure the high impedance and low loss factors of

dielectric materials over a broad frequency range but also accurately compute extremely conductive materials with low impedance.

3.2.3 Faraday Cage

Figure 3-3: Faraday cage setup

The dielectric tests, however, are performed in an enclosed Faraday cage, shown in the figure above while being connected to an alpha analyzer. This prohibits the interference of any external electromagnetic fields. The samples were placed between two copper electrodes attached to a polycarbonate block which acts as a holder for the electrodes shown in the figure below.

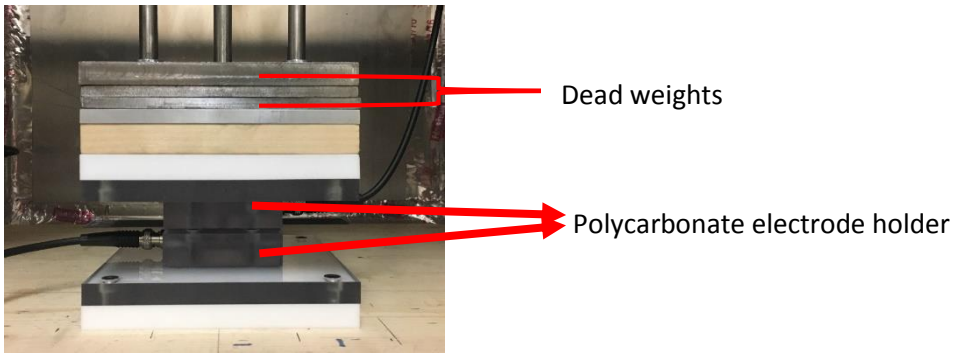

Figure 3-4: Dead weights and polycarbonate electrode holder arrangement inside a Faraday cage

All the measurements were performed using a 0.5” (12.7 mm) circular electrode. The electrodes were cut and polished with fine grit sandpapers before performing the tests. Therefore, there is a variation in results that occur due to the polishing. The figure below shows the deviation of the real part of the permittivity with the diameter of the electrode.

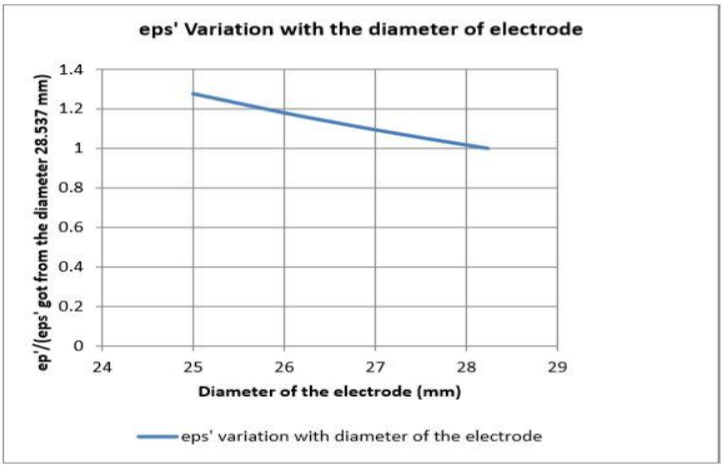

Figure 3-5: Change in the real part of permittivity with varying electrode diameter [14]

Additional weight was added to the electrode in the form of dead weights shown in the figure above. And, the dielectric properties were measured. The plot below shows the increase in dielectric properties with increasing pressure.

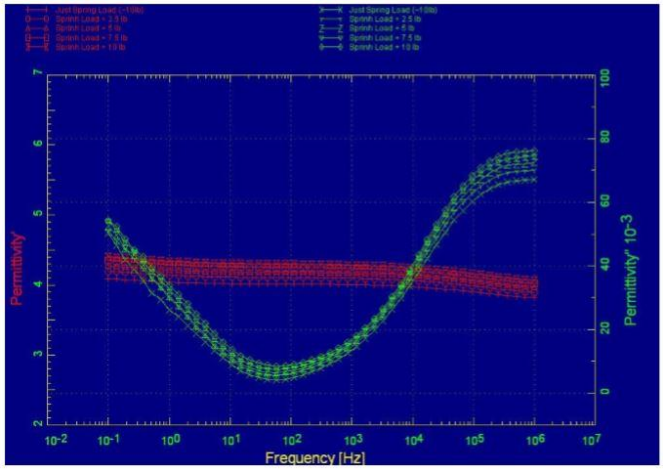

Figure 3-6: Change in the electrode pressure with varying dielectric properties [14]

Moreover, each specimen was tested several times for its repeatability, eligible up to five tests per specimen. After each test, the specimen was kept outside of the Faraday cage for approximately ten minutes. The specimens were usually tested in an alternate fashion wherein a set of specimens was tested followed by the next set. Finally, when the final graph was plotted for all the tests, a close accordance was established between the results plotted as shown in the figure below.

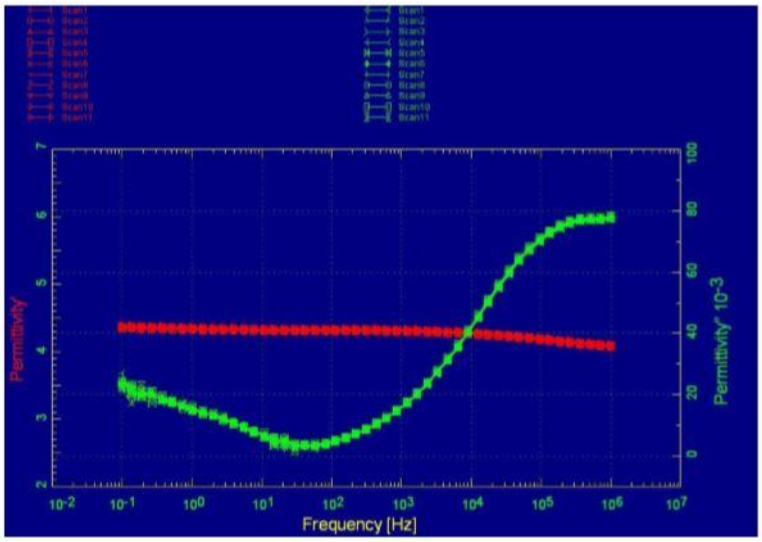

Figure 3-7: Test of repeatability [14]

The figure shows the circuit of the Broadband Dielectric Spectrometer linked with the Faraday cage.

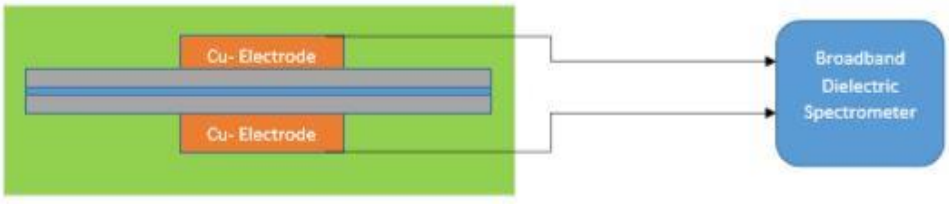

Figure 3-8: Faraday cage linked with BbDS setup

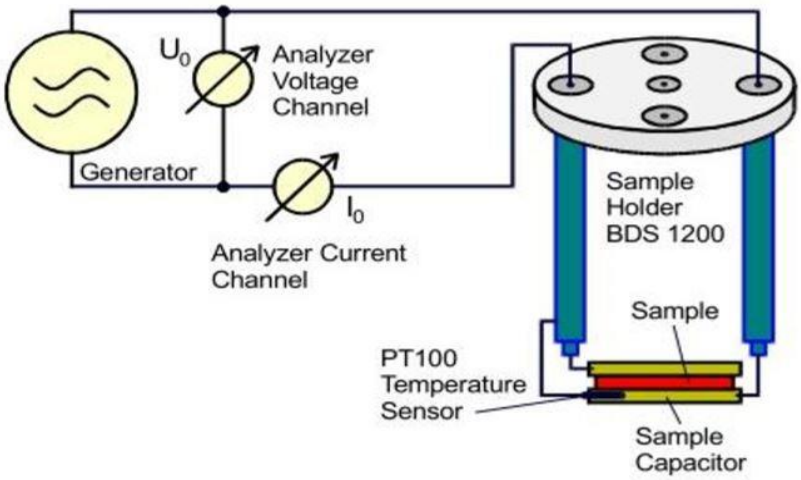

Figure 3-9: Dielectric measurement principle

A voltage U_0 with a fixed frequency $\frac{\omega}{2\pi}$ is applied to the sample capacitor, U_0 causes a current I_0 at the same frequency in the sample. In addition, there will generally be a phase shift between current and voltage described by the phase angle φ.

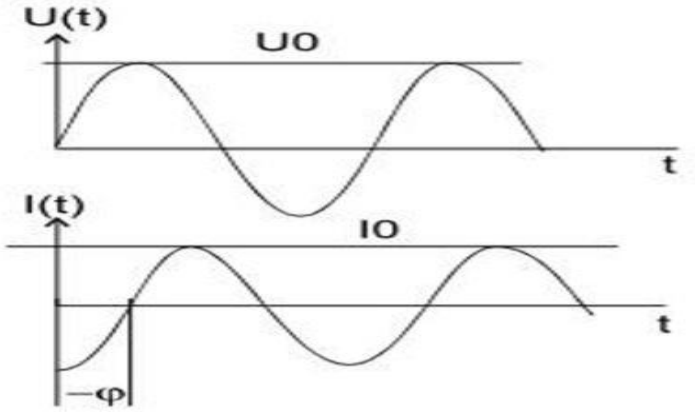

Figure 3-10: Amplitude and phase relation between current and voltage of a sample capacitor

The ratio between U_0 and I_0 and the phase angle φ are determined by the material's dielectric properties (permittivity and conductivity) as well as the specimen's geometry. Thus, the suitable relations in complex form is given as

$$\mathrm{U(t)} = U_0 \cos(\omega t) = \mathrm{Re}\,(U^* \exp(i\omega t)) \tag{11}$$

$$\mathrm{I(t)} = I_0 \cos(\omega t + \varphi) = \mathrm{Re}\,(I^* \exp(i\omega t)) \tag{12}$$

With,

$$U^* = U_0 \tag{13}$$

$$I^* = I' + I'' \tag{14}$$

$$I_0 = \sqrt{I'^2 + I''^2} \tag{15}$$

$$\tan\varphi = \frac{I''}{I'} \tag{16}$$

For a sample with linear electromagnetic response, the measured impedance of the sample capacitor is

$$Z^* = Z' + iZ'' = \frac{U^*}{I^*} \tag{17}$$

And the imaginary permittivity can be calculated by

$$\varepsilon^*(\omega) = \varepsilon' - i\varepsilon'' = \frac{-i}{\omega\, Z^*(\omega)} \cdot \frac{1}{C_0} \tag{18}$$

Here C_0 is the capacity of the empty sample capacitor.

The specific conductivity is related to the dielectric function

$$\sigma^*(\omega) = \sigma' - i\sigma'' = i2\pi f \varepsilon_0 (\varepsilon^* - 1) \tag{19}$$

And electric modulus can be calculated by the equation given below,

$$M^*(\omega) = \frac{1}{\varepsilon^*(\omega)} \tag{20}$$

3.3 Mechanical Response Measurement

An MTS™ Landmark system was used to measure the mechanical strength of the specimens. It provides the required flexibility and duplicity to perform a full range static loading. The adhesive bonded specimens were loaded until failure in a MTS™ Landmark system testing machine of 150 Kn capacity with a loading rate of 50 N/sec.

Figure 3-11: MTS™ Landmark System Universal Testing Machine

Chapter 4

EXPERIMENTAL PROCEDURE

In this case, two different sets of experiments were performed as listed below

1. Dielectric study of adhesive bond with a distinct surface quality for each of the button specimens- The relationship between the surface preparation of the bond-line and its dielectric behavior for 1”x1” button specimens was studied.
2. Bond strength prediction of single-lap joint specimens based on its dielectric behavior- Investigated the variation in mechanical strength with the changing dielectric response of single-lap joint specimens.

The procedure followed for these two experiments are discussed below.

4.1 Dielectric study of adhesive bond with distinct surface quality of button specimens

As discussed earlier, the specimens were prepared using Torayca T700S/G94 carbon fiber prepreg by the compression molding method. This was followed by cutting the 10” x 10” sized laminate into small button specimens of 1”x1” using a shear cutter.

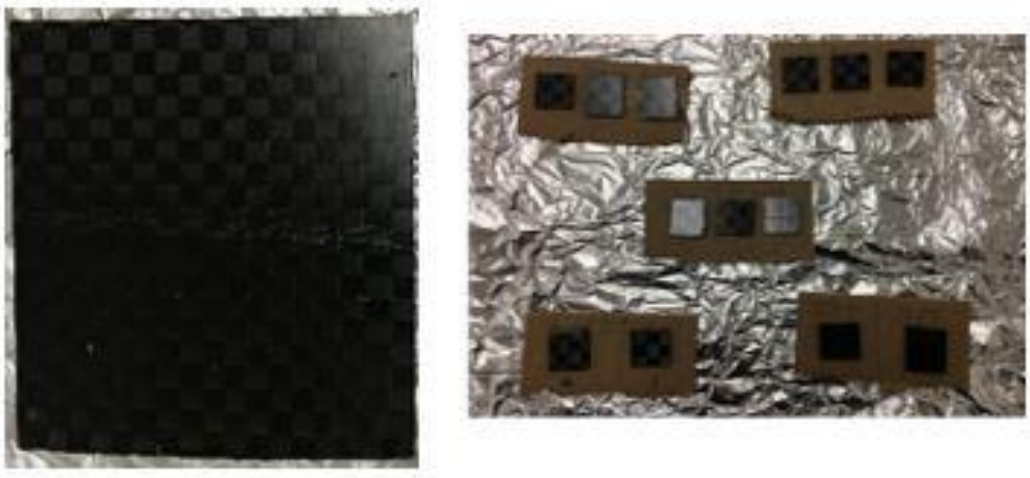

Figure 4-1: Post-manufactured 10” x 10” CFRP laminate (left) and 1” x 1” button specimens cut from the laminate (right)

4.1.1 Specimen Preparation

To develop a bond that replicates a weak adhesive bond, six different groups of specimens were made and the interfacial polarization studied. And, each group comprised of three distinct samples. The differentiating feature between these specimen groups was that the surface of each of these specimens was treated differently as given below. ASTM D2093-03 (2011) standard was followed for the various surface treatment methods.

1. Specimen A - The specimen was sanded on both surfaces of the joint
2. Specimen B - Only one surface of the specimen was sanded.
3. Specimen C - The specimen was not sanded on any surface.
4. Specimen D - The specimen was prepared with a water drop on an unsanded surface
5. Specimen E - The specimen was completely immersed in water before bonding as shown in the figure below.
6. Specimen F - The specimen was prepared with oil drop on one surface.

Figure 4-2: Specimen A (left) and Specimens D and E (right)

4.1.2 Adhesive Bond Preparation

These button specimens were then bonded using an aerospace grade adhesive, in this case, Henkel Hysol EA9394 which is a two-part epoxy adhesive. This was formulated by mixing 50 grams of Part A with 7 grams of Part B under a fume hood based on manufacturers requirements. The adhesive bond line thickness was maintained by introducing glass microspheres in the two-part epoxy mixture. Thus, the final thickness of the bond turned out to be around 0.03 inches. The figure below shows an adhesive bonded button specimen.

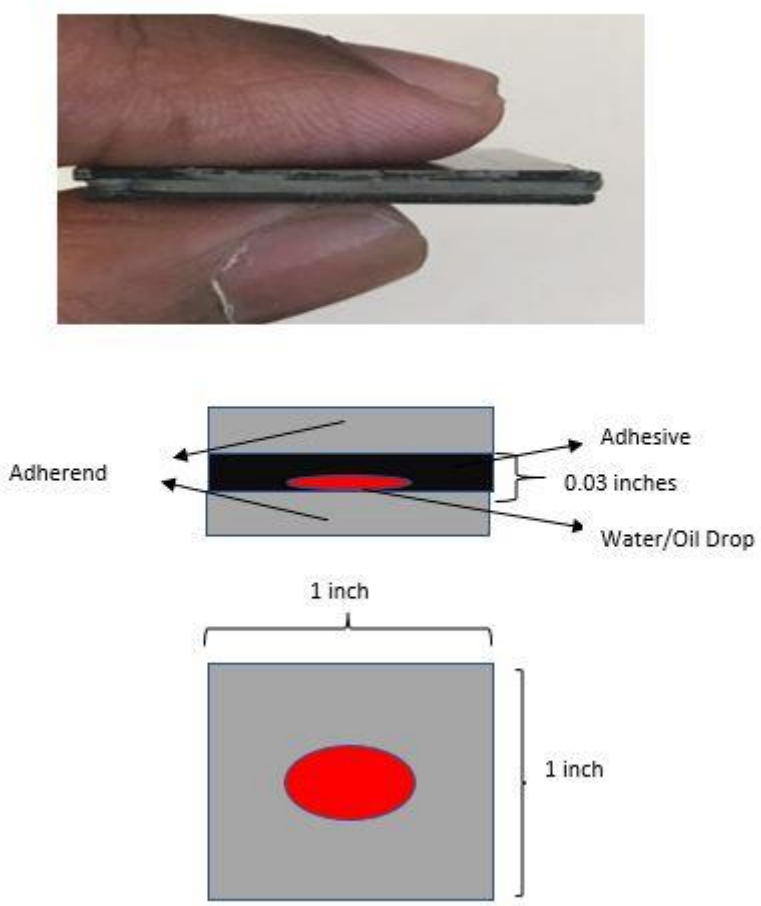

Figure 4-3: Adhesive bonded button specimen (top) and schematic of the same (bottom)

4.2 Bond strength prediction of single-lap joint specimens based on its dielectric behavior

The single-lap joint specimens, were manufactured using the same raw materials that were used for the button specimens as discussed earlier i.e. Torayca T700S/G94 carbon fiber prepreg. However, the laminate was cut into 4”x1” specimens post-manufacture.

4.2.1 Specimen Preparation

As shown in the figure below, the single-lap joint specimens were made using ASTM D5868-01 (2014). In this case, four different groups of specimens were made with varying surface quality listed below.

1. Specimen A - The specimen was sanded on both sides without any inclusions.
2. Specimen B - The specimen was prepared with a water drop on one of the two sanded surfaces.
3. Specimen C - The specimen was prepared with an oil drop on one of the two sanded surfaces.
4. Specimen D - The specimen was prepared with a piece of vacuum bagging film on one of the two sanded surfaces. The size of the film was 0.50” x 0.50”.

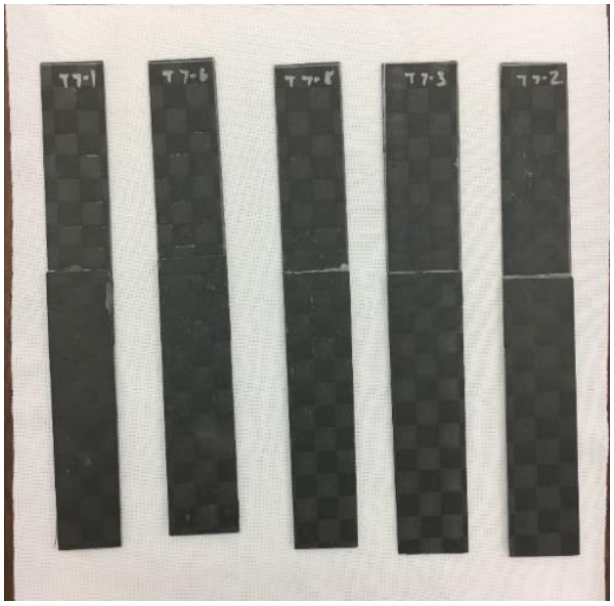

Figure 4-4: Single-lap joint samples for Specimen A

4.2.2 Adhesive Bond Preparation

The single-lap shear specimens were bonded using the same aerospace grade adhesive as used earlier for the button specimens. In this case, glass microspheres were not added to the two-part epoxy mixture, as the total thickness of the bonded joint turned out to be approximately 0.075 inches shown in the figure below.

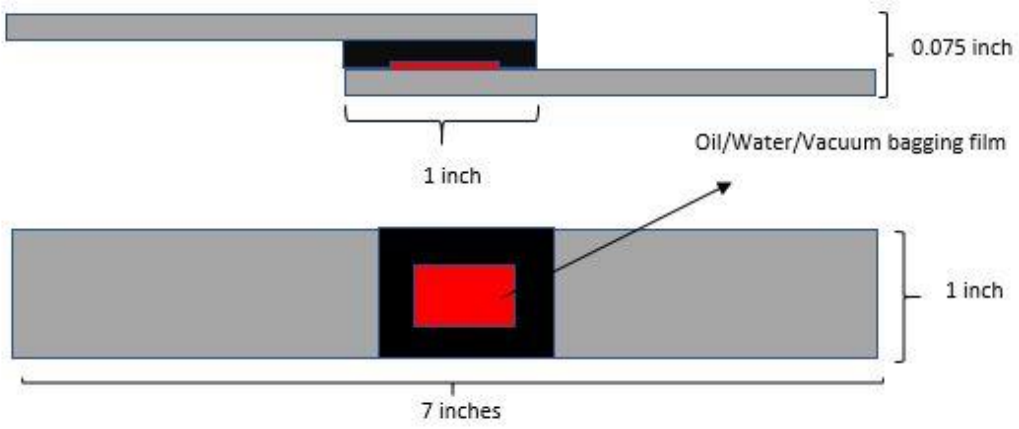

Figure 4-5: Schematic of a single-lap joint specimen

4.3 Dielectric Behavior Analysis

The dielectric measurement of the button and single-lap joint specimens was performed in a Novocontrol™ Broadband Dielectric Spectrometer. Thus, five readings of each sample from each specimen group were carried out. The working principle used for operating the Faraday cage setup is given below.

1. The specimen is placed between the electrode blocks within the Faraday cage, thus forming a capacitor.
2. This is followed by applying a voltage with fixed frequency thus resulting in a flow of current of same frequency.
3. Thus, the dielectric properties of the specimen can be detected with the values of applied voltage and current response.
4. The alpha analyzer measures the complex dielectric function, impedance and conductivity as a function of frequency.

WinDETA by Novocontrol™ is the evaluation software used for the dielectric and impedance measurements.

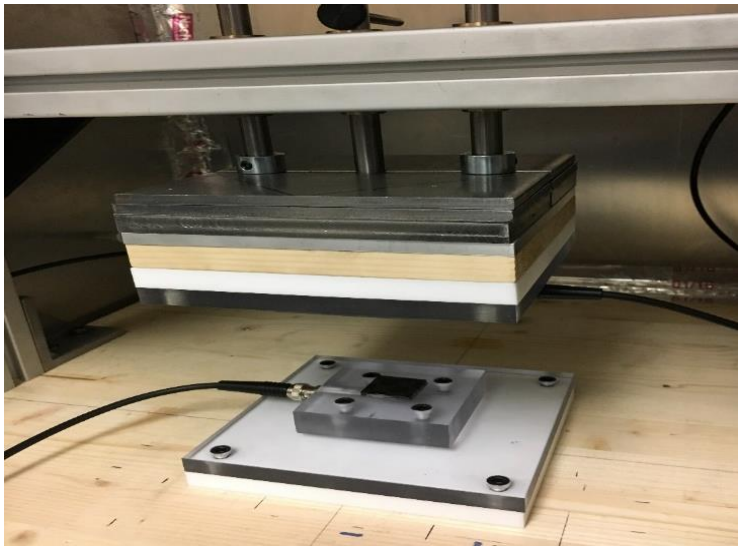

Figure 4-6: A button specimen placed between the copper electrodes

4.4 Mechanical Characterization

The single-lap joint specimens were tested for their mechanical strength as shown in the figure below. MTS™ Landmark Universal Testing Machine was used for performing the tests by computing the breaking load and strain for each sample using MTS TestSuite™ Multipurpose Elite Software. ATM D5868 standard was followed while performing the lap shear tests on the specimens.

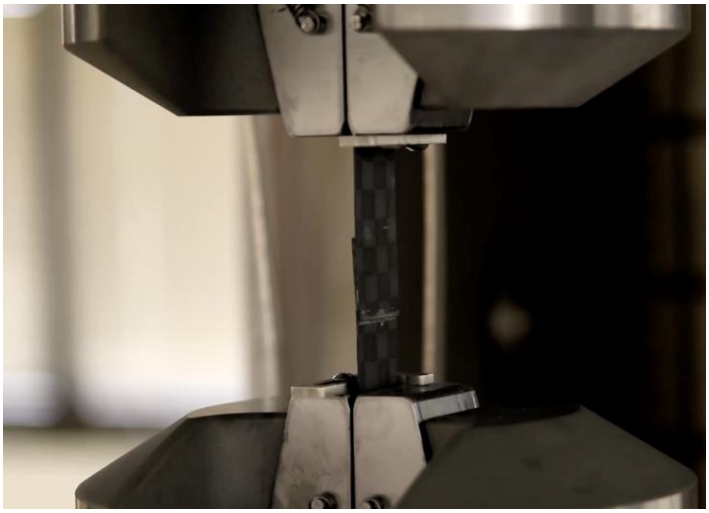

Figure 4-7: Quasi-static loading of a single-lap joint specimen

4.5 Summary

Eighteen button specimens and twenty single-lap joint specimens were manufactured using carbon fiber/epoxy prepreg raw material. These specimens were then bonded using a two-part aerospace grade adhesive. The kissing bond was reproduced by inserting an external inclusion or contaminant in the form of water drop, oil, or a vacuum bagging film. These specimens were then tested for their dielectric properties in a Broadband Dielectric Spectrometer while the single-lap joint specimens were also tested for their mechanical strength in a Universal Testing Machine. Following table shows a list

of quantity of samples made for the two specimen groups and the different contaminants implanted in each of these samples.

Table 4-1: Quantity of bonded composite specimens made and the inclusions used in each of them

Specimen Type	Surface preparation method/ Contamination	Nomenclature	No. of specimens	Tests performed
Button	Both sides sanded	A	3	Dielectric
Button	One side sanded	B	3	Dielectric
Button	No side sanded	C	3	Dielectric
Button	Drop of water on one side	D	3	Dielectric
Button	Specimen was immersed in water	E	3	Dielectric
Button	Drop of oil on one side	F	3	Dielectric
Single-lap joint	No inclusion	A	5	Dielectric/Mechanical
Single-lap joint	Drop of water	B	5	Dielectric/Mechanical
Single-lap joint	Drop of oil	C	5	Dielectric/Mechanical
Single-lap joint	Vacuum bagging film	D	5	Dielectric/Mechanical

Chapter 5

RESULTS AND DISCUSSIONS

The following sections include the dielectric results of all the specimens computed using Broadband Dielectric Spectroscopy method followed by measuring the mechanical strength of single-lap joint specimens. The essential purpose of any non-destructive evaluation method is to approximate the actual strength measured by means of damaging the specimen with any physical, chemical or, in this case, dielectric parameter determined without causing any damage to the specimen. Thus, a correlation was devised between the strength of the adhesive joint and one of the many dielectric parameters observed during the dielectric behavior analysis. This method can be adopted as a benchmark for determining the bond quality for bonds with different surface preparation methods and geometries.

5.1 Broadband Dielectric Spectroscopy

The dielectric behavior analysis of both the button specimens and single-lap joint specimens were carried out as given below. The dielectric properties vary with varying frequency range and thus BbDS proves to be a robust tool for examining the change in material states. Thus, the complex dielectric function $\varepsilon^*(\omega)$ depends on the temperature and angular frequency ($\omega=2\pi f$). The frequency range for collecting dielectric data was 0.1 Hz to 1 MHz. And the dominating polarization mechanisms observed in this range is the interfacial and dipolar polarization.

5.1.1 Button Specimens

To simulate kissing bond, six different types of button specimens were made with varying surface preparation methods as discussed earlier And, the interfacial polarization of the bonded joint was analyzed using BbDS. Three different parameters were taken into consideration for evaluating the experimental data. They are as explained below.

5.1.1.1 Permittivity

Different type of polarization mechanisms has different relaxation levels which are identified by an increase in the imaginary part of permittivity ε" and a stepwise decrease in the real part ε' with increasing frequency. However, the imaginary part of permittivity can also increase with decreasing frequency. This usually occurs when the conduction phenomena or polarization exists at inner boundaries. From equation (8), we have,

$$D = \varepsilon\varepsilon_0\vec{E}$$

In this case, $\varepsilon = (1 + \chi)$ is the permittivity of the material, also known as relative permittivity. Thus, from equation (18) we have,

$$\varepsilon^*(\omega) = \varepsilon' - i\varepsilon"$$

From the above equation, ε' is the real part of the complex permittivity while $\varepsilon"$ is the imaginary part of the same. Thus, two graphs corresponding to the real and imaginary values of permittivity vs. logarithmic frequency values were plotted for each of the button specimens, shown below.

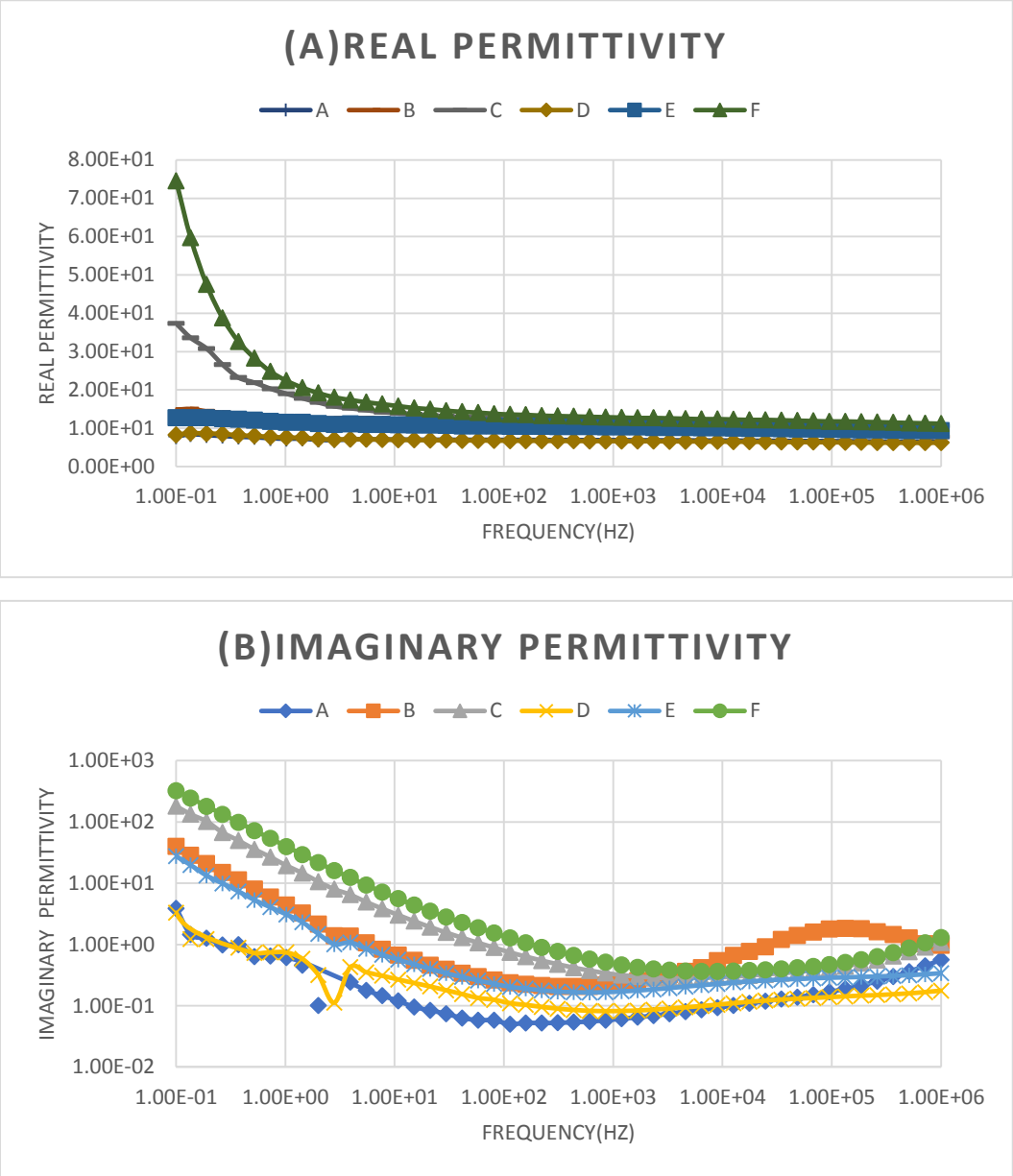

Figure 5-1: (A) Real permittivity vs. Frequency and (B) Imaginary permittivity vs. Frequency [21]

From the above graphs, it's safe to assume that the plot for specimen A has more stability as compared to the other specimens. Thus, it can be a bit troublesome at times to distinguish one specimen from the other.

5.1.1.2 Electric Modulus

From equation (20), we have,

$$M^*(\omega) = \frac{1}{\varepsilon^*(\omega)}.$$

Thus, we can say that the electric modulus is nothing but the inverse of dielectric permittivity. The advantage of electric modulus over permittivity is that it reduces the variations occurring in the higher values of permittivity and conductivity at low frequencies. (Psarras, 2002) (Psarras, 2003). The following graphs show the real and imaginary values of electric modulus vs. logarithmic frequency values for the button specimens

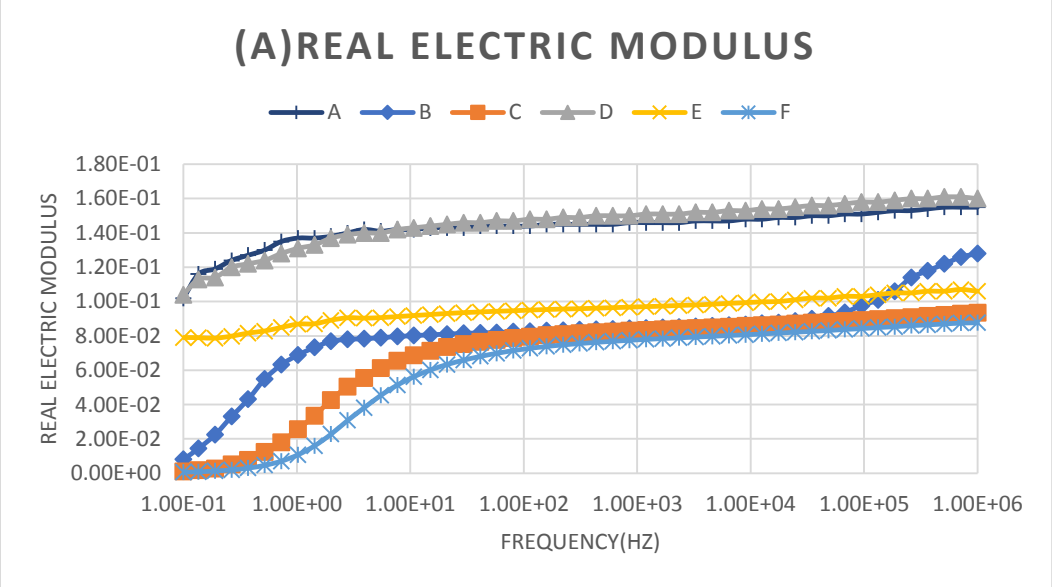

Figure 5-2: (A) Real Electric Modulus vs. Frequency [21]

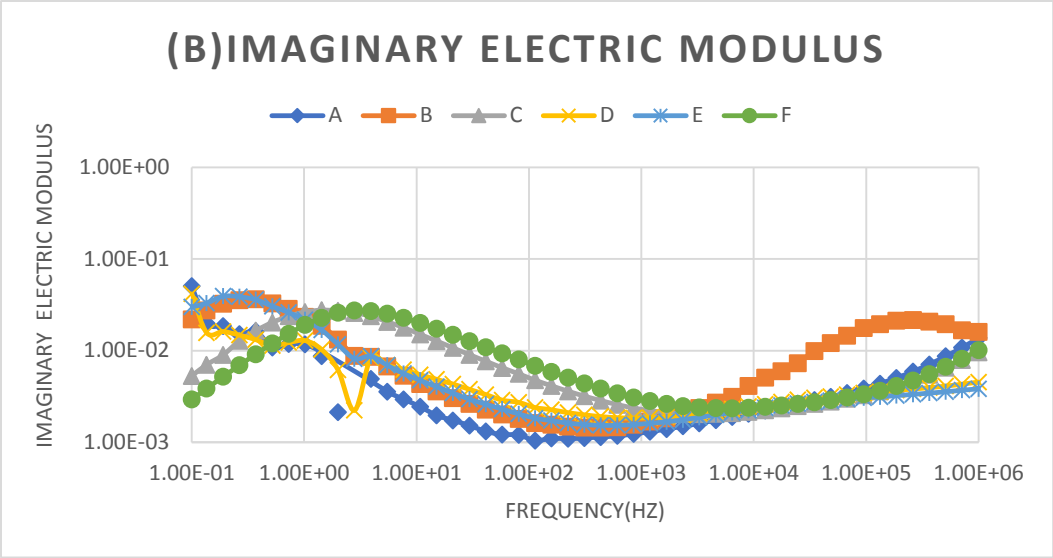

Figure 5-3: (B) Imaginary Electric Modulus vs. Frequency [21]

From the above plots, it's evident that specimen A has the highest real part of electric modulus while it's the lowest for specimen F. This is because specimen F has a higher charge accumulation because of the oil drop in between which acts as an external defect. This ultimately results in a higher interfacial polarization in specimen F as compared to the others. So, the specimens can now be ranked from the least to the most defective given as A – D – E – B – C – F.

5.1.1.3 Dielectric Relaxation Strength

Dielectric Relaxation Strength (DRS), can be defined as the algebraic difference between the static permittivity value and the limiting high-frequency permittivity.

$$\Delta\varepsilon = \varepsilon_0 - \varepsilon_\infty \quad (21)$$

Thus, it proves to be a crucial parameter in establishing the interfacial polarization. Thus, DRS is based on the relation that a heterogeneous composite material has higher level of interfacial polarization if it has a higher DRS. This supports the fact that the greater the defects in a system, the higher is the observed DRS value. The following graph shows

the DRS values of all the tested specimens. These values are however normalized based on the least value of all the measured DRS values.

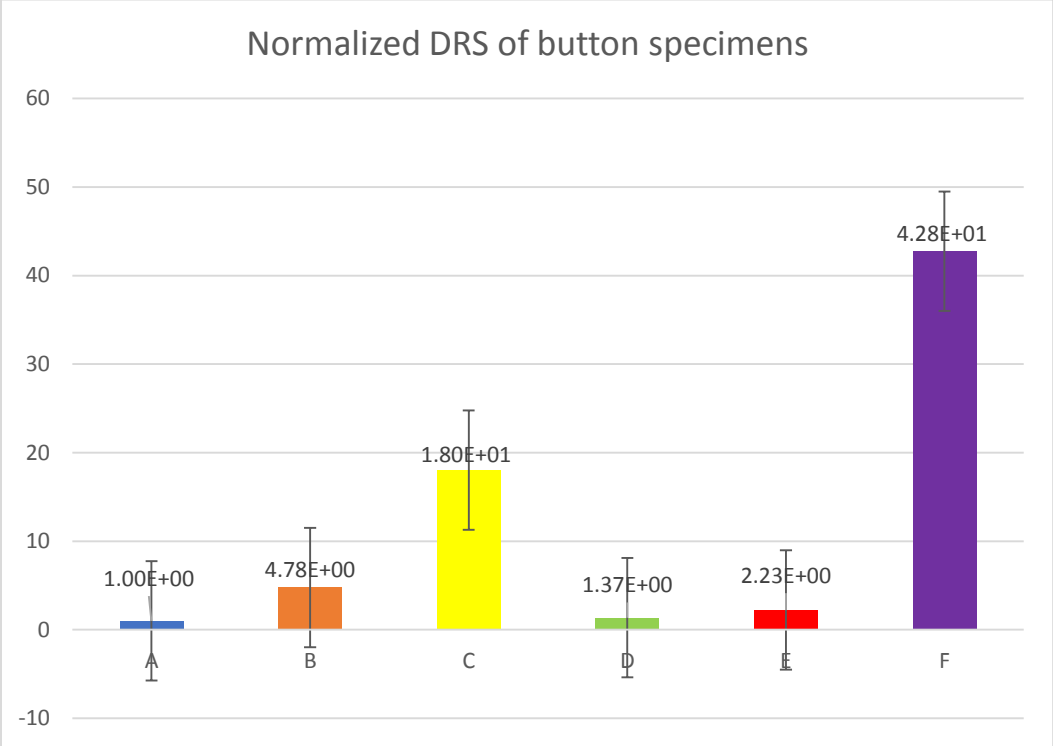

Figure 5-4: Normalized DRS values for button specimens

After observing the DRS values for the button specimens, we can conclude that specimen F has the highest DRS value as compared to the rest of the specimens. This theory is also supported by the values for electric modulus as discussed above. Thus, ranking the specimens at least defective to the most defect, we have A – D – E – B – C – F.

5.1.2 Single-lap Joint Specimens

The kissing bond was replicated by inserting three different materials with varying properties between the interface of the adhesive and the adherend. Thus, four different types of single-lap joint specimens were made of which three had an inclusion between

the interface. The three inclusions were water, oil and vacuum bagging film. However, for the single-lap joint specimens, only one parameter was considered for the dielectric behavior analysis. Thus, the results for this set of experiments are given below.

5.1.2.1 Dielectric Relaxation Strength

The Dielectric Relaxation Strength for the single-lap joint specimens was calculated from the permittivity values observed. The plot for the average values for DRS is as shown below.

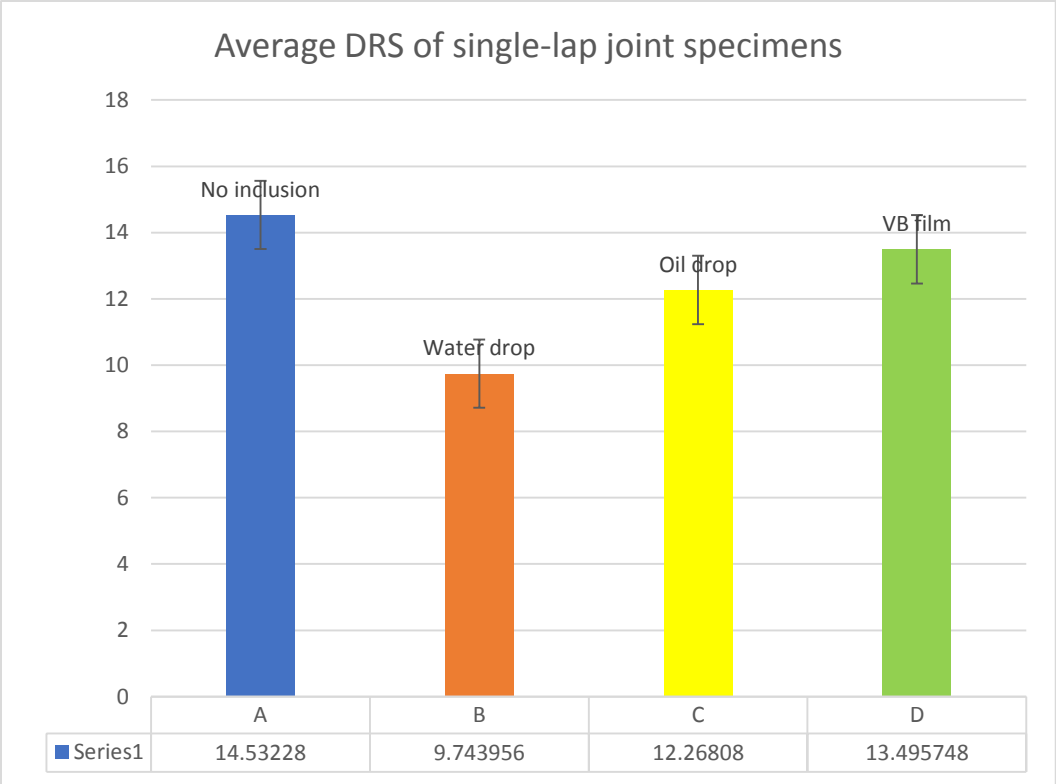

Figure 5-5: Average DRS values for single-lap joint specimens

In the above plot, specimen A has the highest DRS value as compared to the rest of the three specimens. Thus, the interfacial polarization observed is the highest for specimen A followed by D, C and B.

5.2 Tension Testing

The only complication observed while simulating a kissing bond is that it's next to impossible to detect a weak interface between the bond. Thus, it becomes crucial to perform destructive testing, in this case, lap shear test on these bonded specimens to differentiate it from a good bond. The single-lap joint specimens were tested for their breaking/failure load and a relationship was devised between the shear strength and the dielectric relaxation strength. The plot below shows the average of the failure load of all bonded specimens.

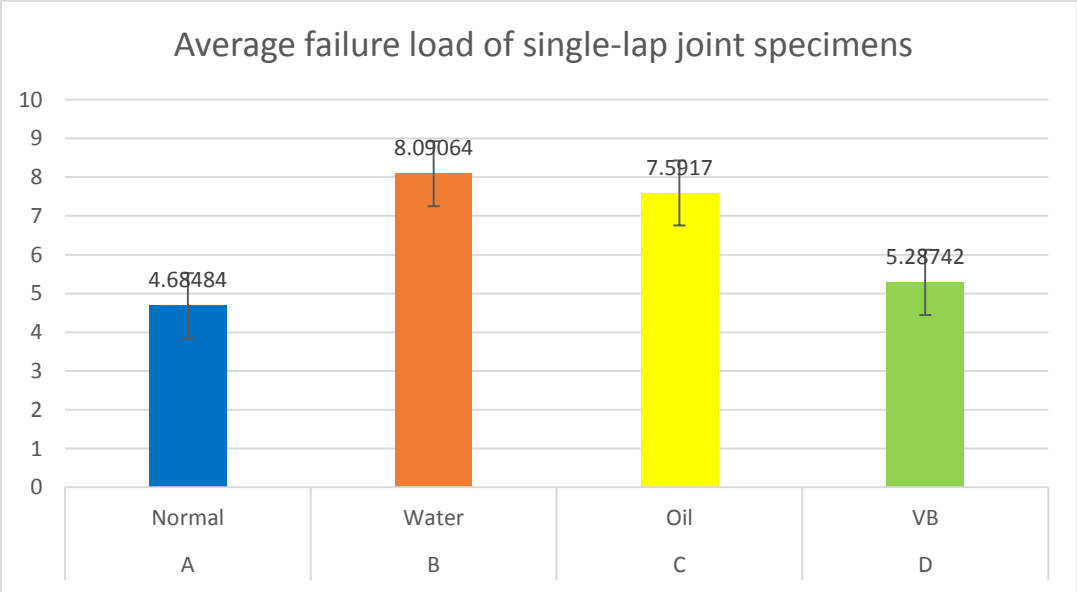

Figure 5-6: Average failure load of single-lap joint specimens

Now, comparing the results obtained from the tensile tests with the DRS values of the single-lap joint specimens, we observe that with increasing DRS the strength to break of the specimen decreases.

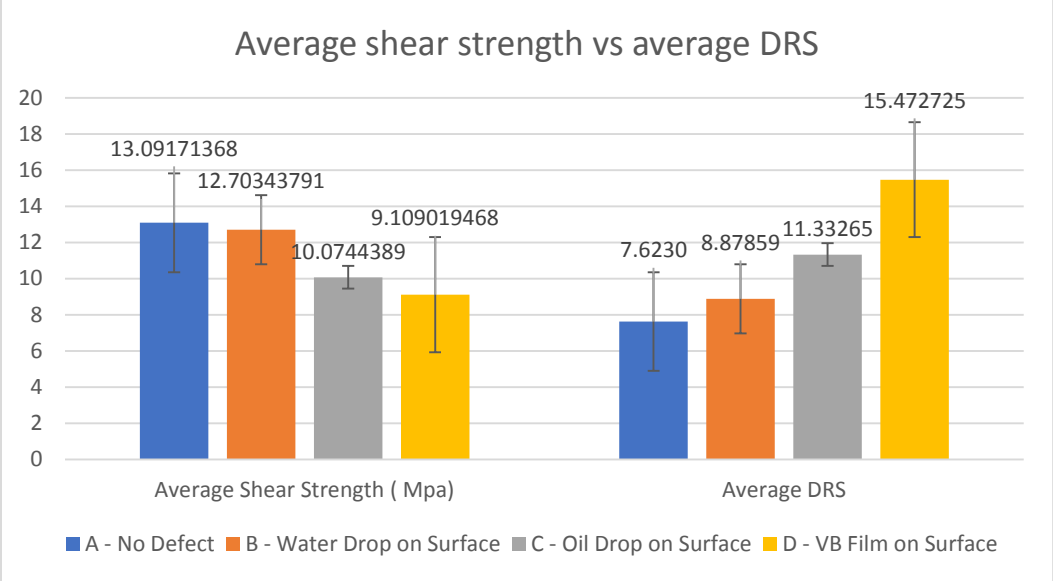

Figure 5-7: Comparison of the shear strength and DRS of single-lap joint specimens [22]

Similarly, normalizing the above values for average DRS and shear strength gave the results as follows.

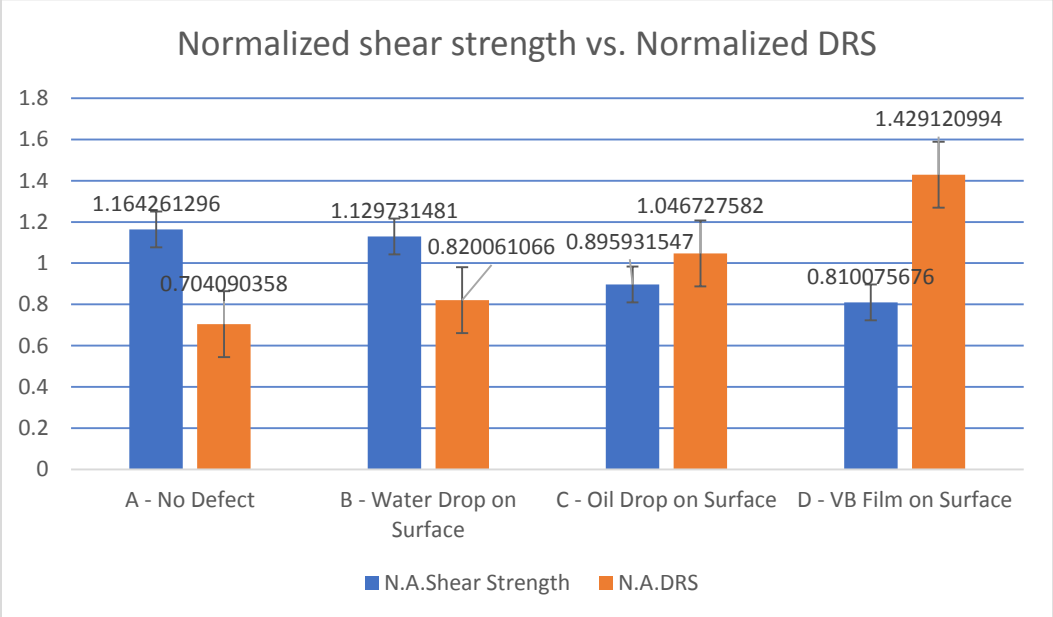

Figure 5-8: Comparison of normalized shear strength and DRS of single-lap joint specimens [22]

In conclusion, the strength of the adhesive bond is found to be higher with a lower DRS value i.e., as the DRS value of bond increases, there is a decrease in its strength.

Chapter 6

FINITE ELEMENT ANALYSIS

A series of FE analysis was performed to validate the results obtained via the experimental method. Thus, a kissing bond model was made in COMSOL software. The AC/DC module of the software was used for performing the analysis. The objective of this study was to observe the difference in the electric potential throughout the bond. A variety of contaminants were used as inclusions while modeling the kissing bond. These were moisture (water). mineral oil and vacuum bagging film (LDPE). The material properties of the various contaminants are listed in the table below along with the properties of the adhesive bond.

Table 6-1: Material properties

Material	Electrical Conductivity (S/m)	Relative Permittivity
CFRP	1000	1
Epoxy Adhesive	1e-14	3.15
Water	5e-5	20
Oil (Shell Diala GX) *	2.39e-12	2.21
Vacuum Bagging Film	1e-6	2.30

The finalized geometry has 6 domains, 23 boundaries, and 18 vertices as shown in the figure below.

Figure 6-1: 2D Model of Adhesive bond

In the above figure, the top and bottom layer is made of CFRP material. And the middle one is a layer of epoxy adhesive. An inclusion is placed between the CFRP and epoxy adhesive layer. Finally, the bonded specimen is fixed between two copper electrodes which are responsible for measuring the through-thickness electrical potential of the specimen. The boundary conditions applied were corresponding to the ones used in the experimental setup. Therefore, the top electrode acted as the terminal with a voltage supply of 1V while the bottom one was grounded.

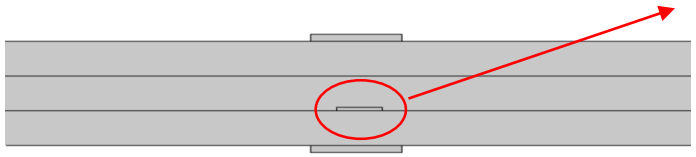

Figure 6-2: Copper electrodes placed on the top and bottom of the specimen with contaminant placed between the carbon and epoxy adhesive interface

A triangular mesh of 1000 elements was generated for the 2D geometry as shown in the figure below. The inclusion used in this case is moisture i.e. drop of water. The electrical potential was measured at three different locations given below.

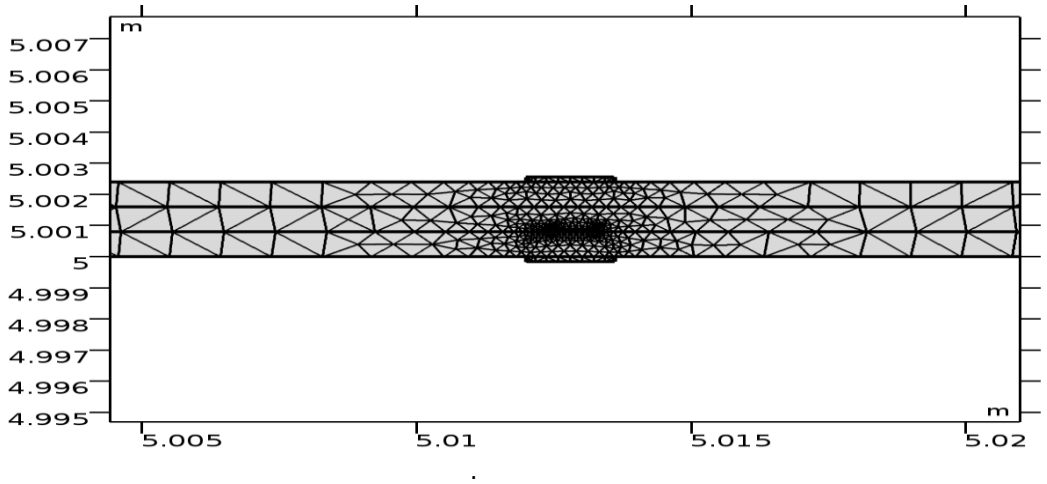

Figure 6-3: 2D mesh of the model with triangular elements

The electric potential was computed at 0.1 Hz for the specimen as shown below.

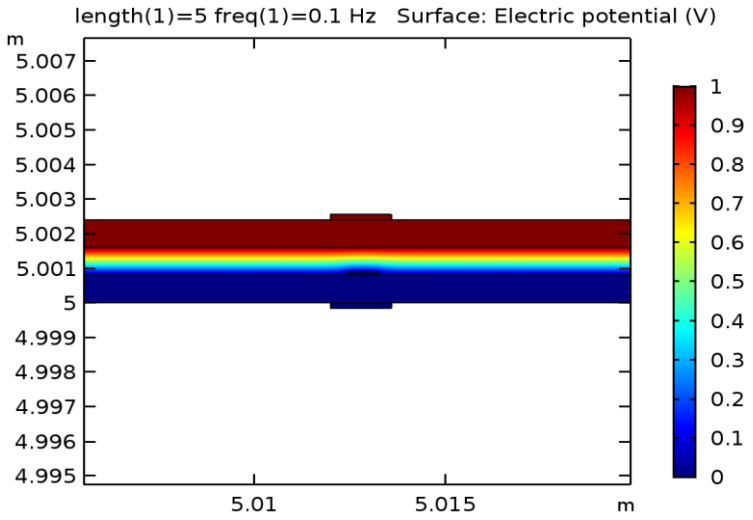

Figure 6-4: Electric potential of the bonded specimen at 0.1 Hz

From the above figure, we see that the electric field decreases through the thickness of the specimen. The electric potential is 1 V in the first layer of the adhesive since carbon is a good conductor of electricity. Th epoxy adhesive, on the other hand, being a poor conductor brings the electric potential to 0 V as it progresses through the specimen. In this case, the drop of water acts as a dielectric and thus charge accumulation occurs resulting in interfacial polarization. This helps us to decide whether a kissing bond is existing in that bonded specimen. Next, the electric potential was computed for three different locations in the specimen over a broad frequency ranging from 0.1 Hz to1 MHz as shown.

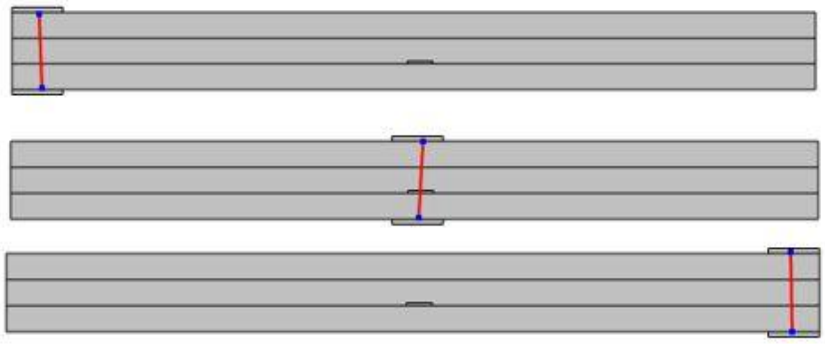

Figure 6-5: The three locations at which the electric field potential was measured

The following graphs show the location as well as the electrical potential measured for that specific location in form of a line graph.

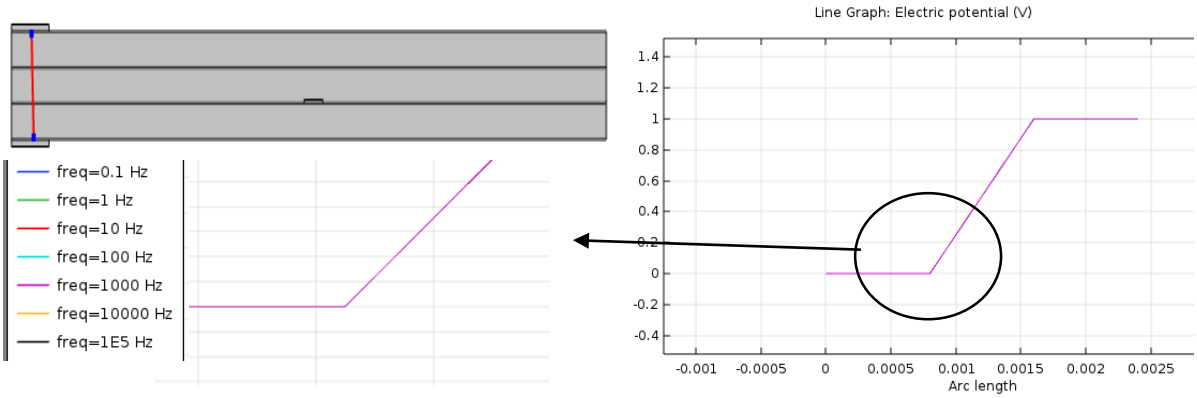

Figure 6-6: Straight line graph for electric potential is observed at a no-defect location

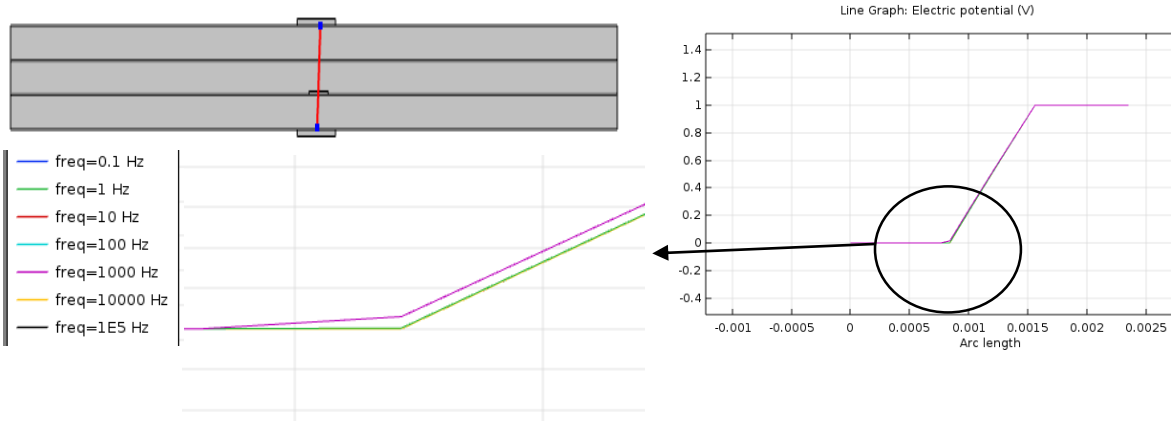

Figure 6-7: Variation in line graph for electric potential is observed at the defect location

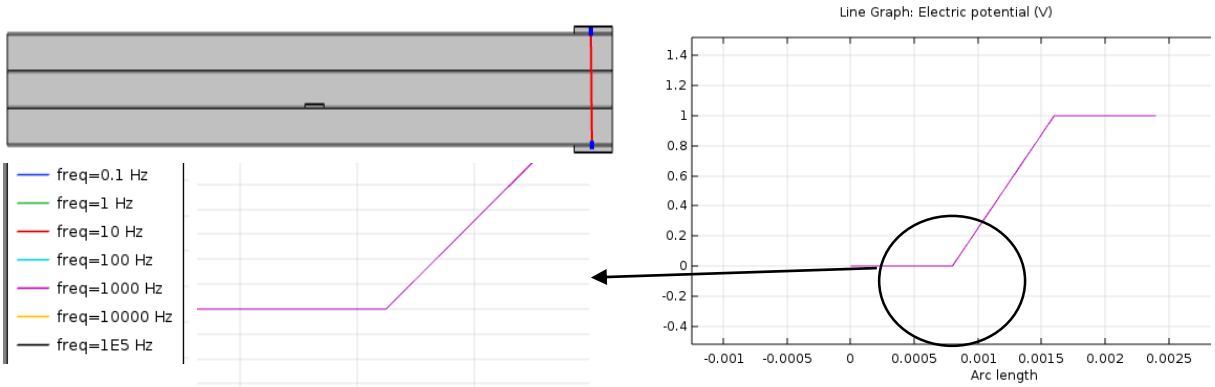

Figure 6-8: Straight line graph for electric potential is observed at a no-defect location

From the above plots, we observe that the electric potential (V) is distinct at each point in the specimen. Thus, comparing the values of electric potential (V) at different locations cam gives us an idea as to where is the defect is located in the specimen.

Similar results are observed for the other two types of contaminants – oil drop (mineral oil) and vacuum bagging film.

6.1 Summary

Thus, we can conclude that the plot for electrical potential varies with respect to frequency throughout the bonded specimen. Thus, we can predict the location of a kissing bond using Broadband Dielectric Spectroscopy.

Chapter 7

HYBRID COMPOSITES

Traditionally, composites are made of two different material systems (usually carbon fiber and a polymer matrix) which are combined on a macroscopic scale. This contributes to a higher strength and stiffness as well as a better fatigue life compared to metals. Hybrid composites, on the other hand, offer an effective way of increasing ultimate strain and impact properties while reducing the cost of a traditional composite material. A great deal of experimentation and investigation has been done in predicting the hybrid nature or mechanical behavior of these hybrid composites. Similarly, a plethora of characterization methods is available to predict the life of hybrid composites which includes both destructive and non-destructive evaluation. Broadband Dielectric Spectroscopy is one such tool that can be used for prognosticating the damage occurring in a material. Moreover, the amount of research done in studying the dielectric aspects of hybrid composites is next to nothing.

7.1 Motivation and Background

As discussed earlier, there are very few NDE methods available to detect any kind of defect or irregularity within a polymer composite be it hybrid polymer composite. Broadband Dielectric Spectroscopy can be used a characterization method to predict the location of interfacial defects in a specimen. This compared with the values obtained via mechanical testing can ultimately be used to predict the life of hybrid composites. Thus, BbDS shows the level of interfacial polarization in a specimen which can further give us an idea about the Dielectric Relaxation Strength of the specimen.

7.2 Literature Review

The most commonly used reinforcement fibers in the business of composites are carbon and glass and thus the most popular hybrid composites are a mix of the two. They initially came into being during the early sixties, to reduce the cost incurred in manufacturing plain carbon fiber composites. The figure below shows the stress-strain diagram of a hybrid composite [26].

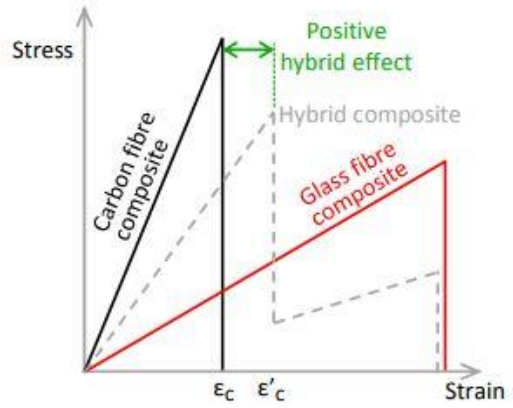

Figure 7-1: Stress-strain diagram of a hybrid composite and corresponding reference composites [26]

Experiments were carried out on inter-ply hybrid composite specimens using satin weave carbon fabric and plain weave E-glass fabric. The 4-ply specimens were made by placing glass fabric on the top and bottom layers while the woven carbon fabric was placed in the center. This was followed by performing in-plane tensile and compressive tests on a quasi-static loading machine. The outcome of this research proved that hybrid composites are more advantageous as compared to normal polymer composites. The reason being hybrid composite specimens have better methods of improving the ultimate strain while lowering the cost at the same. Moreover, hybrid composites have enhanced impact properties than the others [27].

Swolfs et al presented a more effective technique for enhancing the ultimate strain and impact properties. This was done by introducing a small percentage of E-glass or Kevlar in the specimen. The high modulus fibers contributed to high stiffness and load bearing qualities whereas the low modulus fibers, on the other hand, provide resilience to damage occurred while maintaining a low material cost [28].

7.3 Experimental Procedure

In this case, multiple in-house hybrid composite specimens were manufactured and their dielectric behavior analyzed. Each of these 4-ply specimens was implanted with an impurity between the middle two plies. The specimens were then tested for their shear strength and a correlation was realized between the Dielectric Relaxation Strength and shear strength of the specimen.

Two different hybrid composite specimens were made using unidirectional glass-carbon fabric and the other had woven glass-carbon layup. Both these hybrid 4-ply specimens had the same layup with glass fabric on the top and bottom while carbon fabric in the middle. These test specimens were manufactured in-house using compression molding in a Wabash Vantage Series Hydraulic Press and followed the same layup method as used earlier for the adhesive bond specimens. Since two different material systems were used for manufacturing the specimens both materials had a different temperature of cure. So, for manufacturing the hybrid specimens the cure cycle for carbon fiber prepreg was chosen because it had a higher curing time of 120 minutes as compared to the glass fiber prepreg which is 90 minutes. Four different types of impurities were used – vacuum bagging film, paper, Polytetrafluoroethylene (PTFE) and Aluminum. Five samples were made for each of these defective specimens. However, some of these break post-manufacture and were thus discarded from future use. Given below is the experimental

procedure followed while manufacturing the two different types of hybrid composite specimens. The table below shows the different hybrid composite specimens manufactured and the impurity implanted in each of them.

7.3.1 Hybrid unidirectional composites

The following figure shows the layup for unidirectional hybrid composite specimen vacuum bagging film as inclusion.

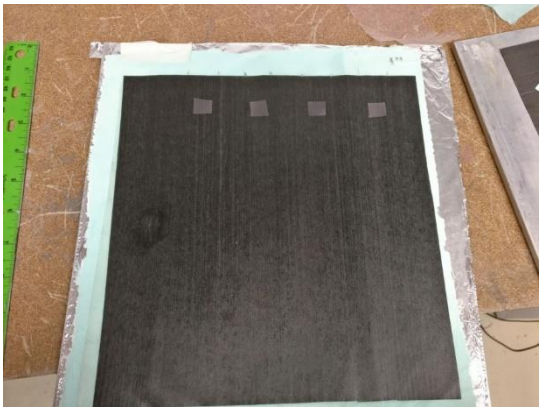

Figure 7-2: Layup of hybrid unidirectional composite with vacuum bagging film as an inclusion/defect

The glass fiber prepreg used in this case is unidirectional E-glass supplied by Rockwest Composites. The layup orientation of the laminate was [0/90/90/0] with the glass fabric placed in the 0-direction on the top and bottom layers whereas the carbon fabric was placed in 90 in the middle two layers. The size of the laminate before it was cut into samples of 6" x 1" was 10" x 10". The samples were cut in 0^0 from the specimen using a tile cutter. However, various problems occurred during the manufacturing process which led to warping and uneven resin flow in the specimen as shown in the figure below.

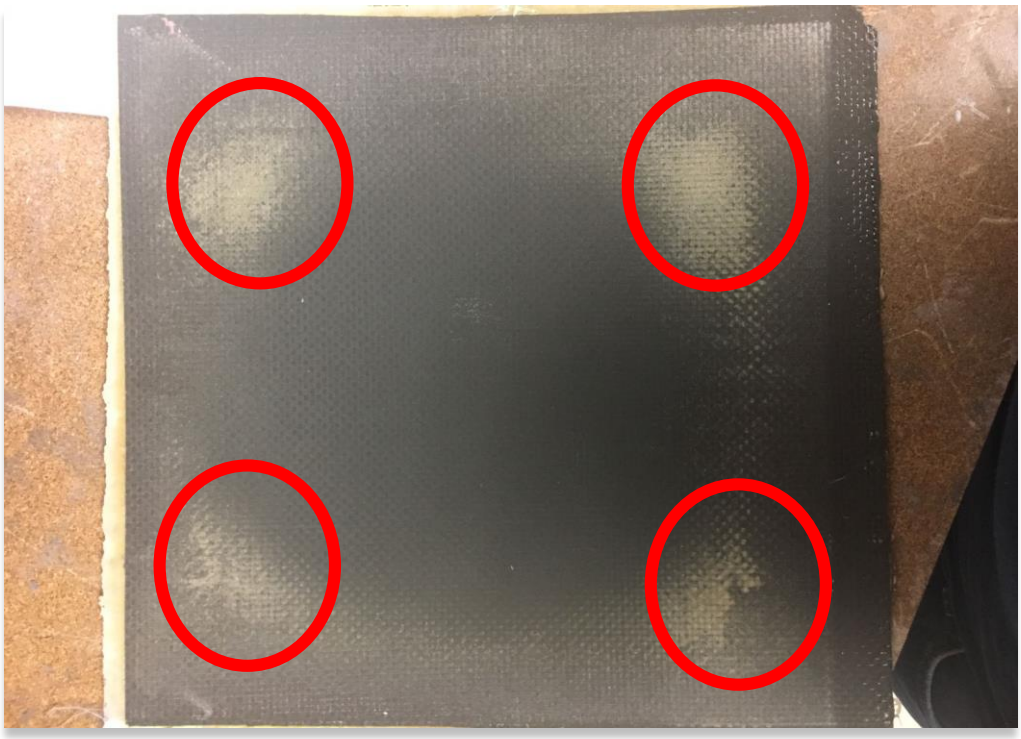

Figure 7-3: Post-cured hybrid woven composite specimen with non-uniform resin flow.

Thus, a majority of the samples were discarded from further analysis which was the ones with PTFE inclusions and the ones without any in the case of unidirectional specimens. The different contaminants used as inclusions for the unidirectional hybrid composite specimens are listed below.

1. Aluminum – The specimen was prepared with Aluminum as an inclusion placed in the center. The size of the inclusion is 0.5” x 0.5”.
2. Vacuum Bagging Film – The specimen was prepared with vacuum bagging film as an inclusion placed in the center. The size of the inclusion is 0.5” x 0.5”.
3. Paper – The specimen was prepared with paper as an inclusion placed in the center. The size of the inclusion is 0.50” x 0.50”.

A set of hybrid unidirectional specimens with aluminum inclusion is shown in the figure below.

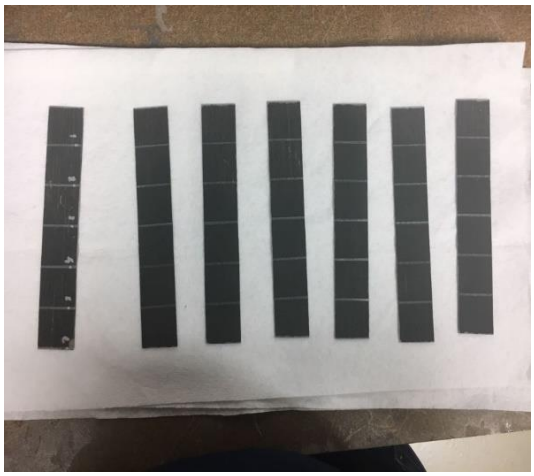

Figure 7-4: Hybrid unidirectional composite samples with aluminum defect

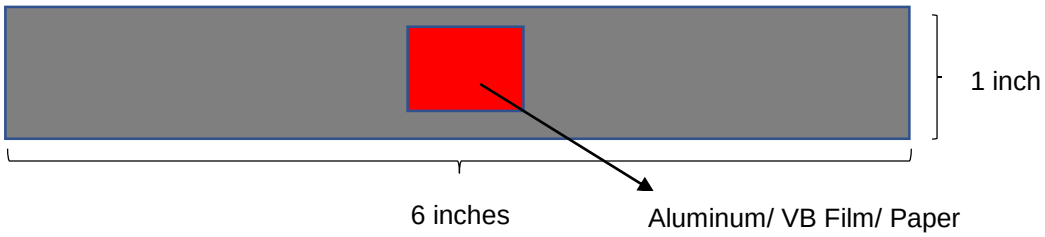

Figure 7-5: Schematic of hybrid unidirectional composite specimen and the types of defects implanted

7.3.2 Hybrid woven composites

The figure below shows the layup for hybrid woven composite specimen with vacuum bagging film as inclusion.

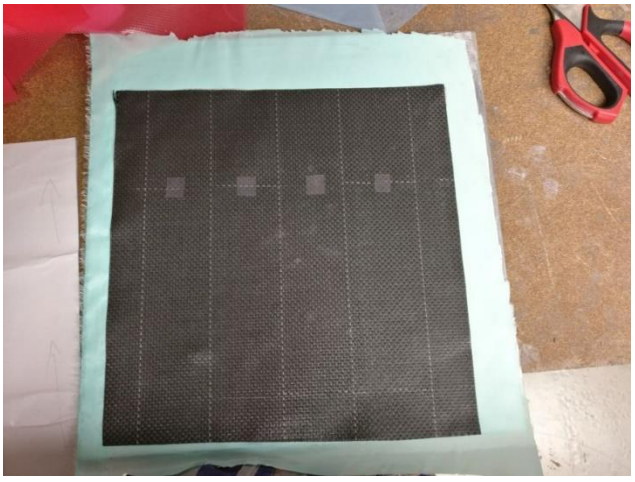

Figure 7-6: Layup of hybrid woven composite with vacuum bagging film as an inclusion/defect

The woven hybrid specimens followed the same layup structure as used in the case of unidirectional specimens. Therefore, the top and bottom layers were made of woven glass fabric while the middle two layers had carbon fabric in them. Although, the layup orientation of the laminate was $[0]_4$ with 0^0 being the warp direction. In this case, as well, many specimens were discarded post-manufacture. These included the specimens with Aluminum and PTFE inclusions. So, the contaminants used as inclusions for the woven hybrid composite specimens are as follows.

1. Virgin – The specimen was prepared without any inclusions between the plies.
2. Vacuum Bagging Film – The specimen was prepared with vacuum bagging film as an inclusion. The size of the inclusion being 0.5” x 0.5”.

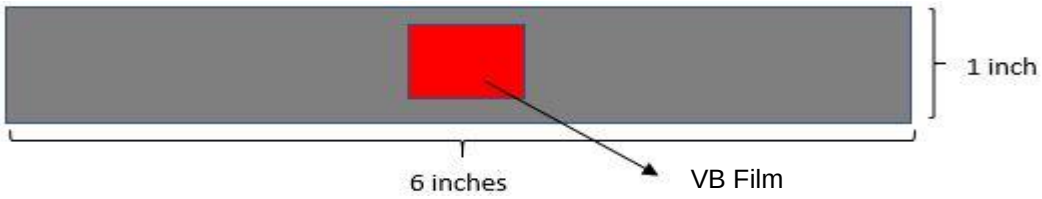

Figure 7-7: Schematic of hybrid unidirectional composite specimen with VB film

The table below shows the quantity of samples made for each of the two kinds of hybrid composite specimens and the inclusions filled in each sample.

Table 7-1: Quantity of hybrid composite specimens made and the inclusions used in each of them

Type of specimen	Inclusion	Nomenclature	Quantity of samples made
Unidirectional	Aluminum	Al	4
Unidirectional	Vacuum Bagging Film	VB Film	4
Unidirectional	Paper	Paper	4
Woven	None	Virgin	4
Woven	Vacuum Bagging Film	VB Film	4

7.4 Results and Discussion

After both the hybrid composite specimens were manufactured, they were assessed for their dielectric behavior using Broadband Dielectric Spectroscopy. The parameter considered for measuring the dielectric behavior was Dielectric Relaxation Strength which is nothing but the algebraic difference between static permittivity value and the limiting high-frequency permittivity as shown in equation (21). This was followed by testing these specimens for their shear strength in a tensile testing machine by applying quasi-static loading. Now, a correlation was tried to establish between the mechanical and the dielectric behavior of the material.

7.4.1 Broadband Dielectric Spectroscopy

The frequency at which the dielectric values, in this case, the real values of permittivity were obtained, ranges from 0.1 Hz to 1MHz. This was followed by plotting the average Dielectric Relaxation Strength (DRS) of all samples for the two hybrid composite specimens – unidirectional and woven.

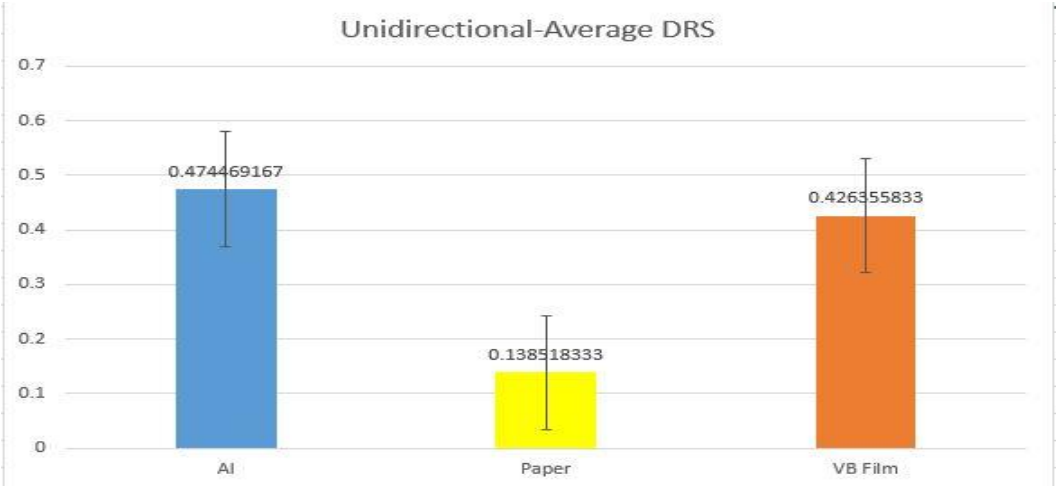

Figure 7-8: Average DRS for hybrid unidirectional composite specimens

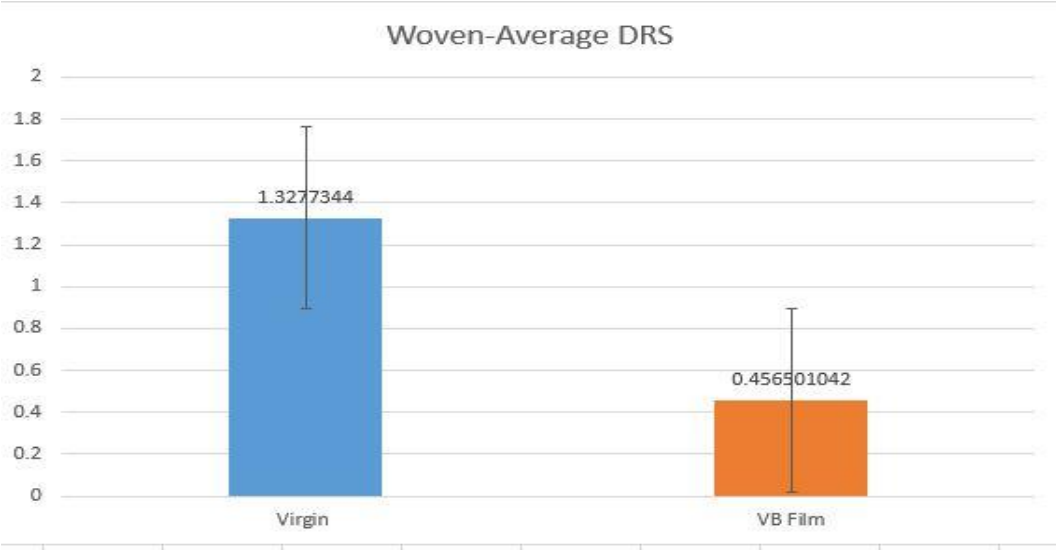

Figure 7-9: Average DRS for hybrid woven composite specimens

7.4.2 Tensile Testing

The unidirectional and woven hybrid composite specimens were then inspected for their failure load. Following plots shows the average breaking load for both hybrid unidirectional and woven composite specimens.

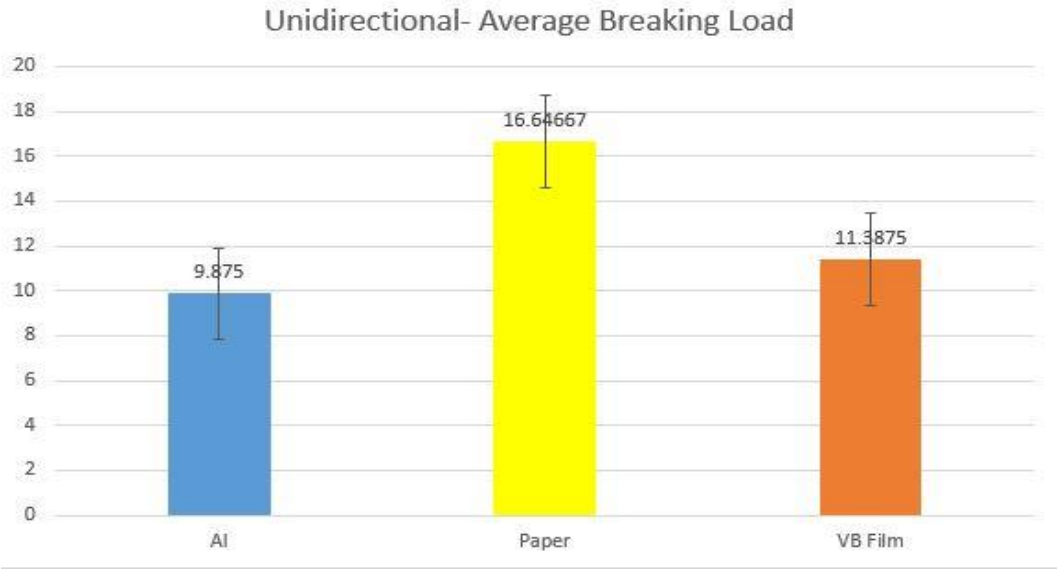

Figure 7-10: Average breaking load for hybrid unidirectional composite specimens

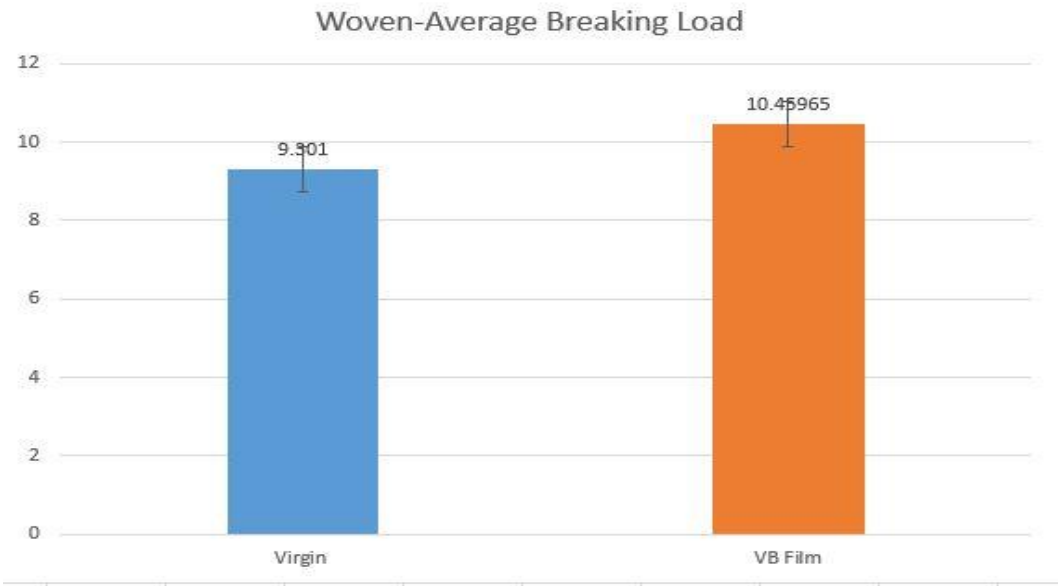

Figure 7-11: Average breaking load for hybrid woven composite specimens

7.5 Summary

From the above plots, it was observed that as the Dielectric Relaxation Strength (DRS) of a hybrid composite specimen is inversely proportional is to failure/breaking load which ultimately is the shear strength of the specimen. The shear strength of a specimen is given by the equation,

$$\tau = \frac{P_{max}}{A} \tag{22}$$

where, τ is the shear strength, P_{max} is the maximum breaking load and A is the average cross-sectional area of the specimen. This can be explained by the plots shown below.

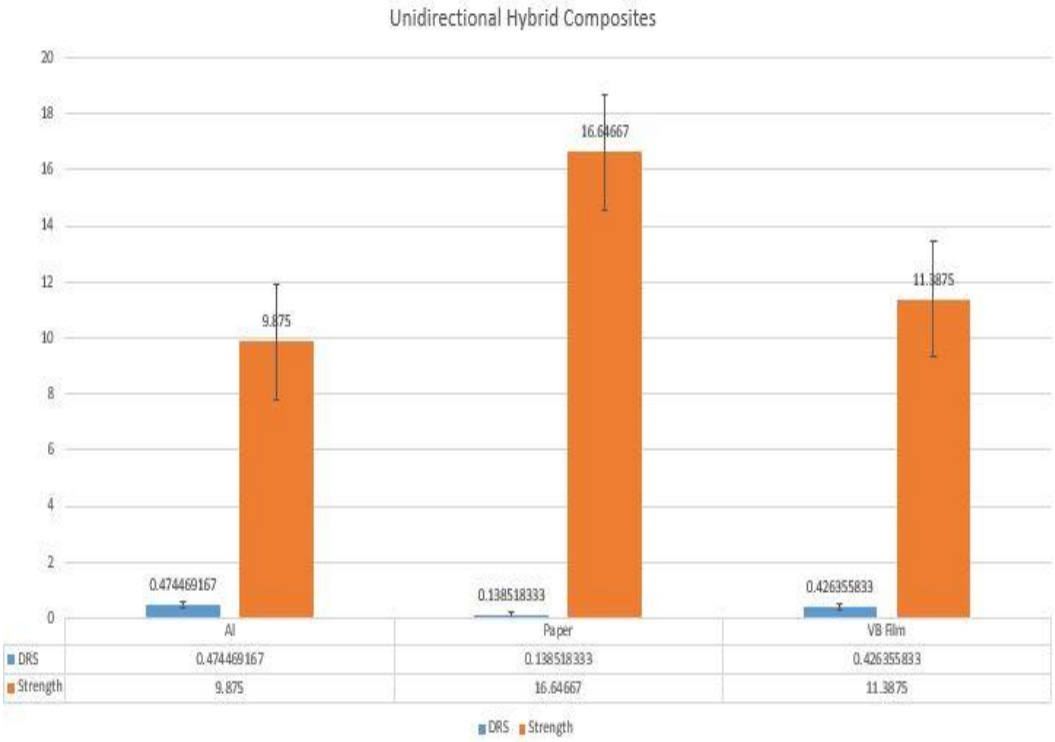

Figure 7-12: Relationship between average DRS and the average shear strength for the hybrid unidirectional composites

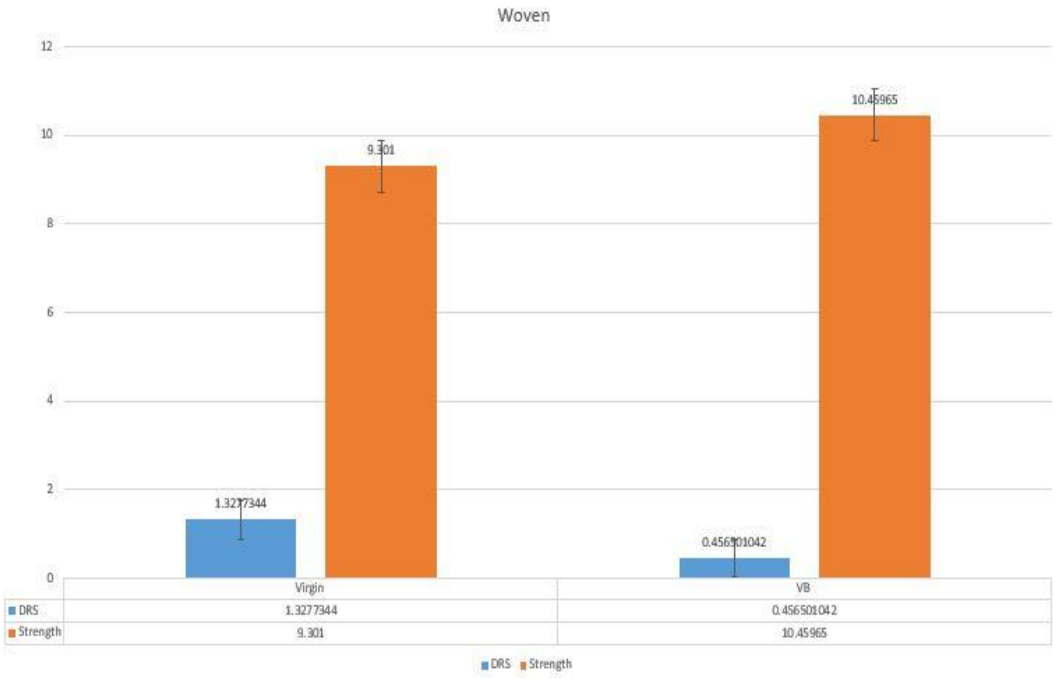

Figure 7-13: Relationship between average DRS and the average shear strength for the hybrid woven composites

Thus, it is proved that Dielectric Relaxation Strength can be used as a parameter to compare the quality of the specimen as proved earlier for adhesive bond. The higher the DRS, the higher is the interfacial polarization in the specimen.

Chapter 8

CONCLUSIONS

From the above experiments, it can be concluded that Broadband Dielectric Spectroscopy can be used as an indicator to detect the bond quality of a specimen. Dielectric Relaxation Strength proved to be a definitive parameter as it is associated with the permittivity values at high and low frequencies. Finally, the outcome of this research was to establish DRS as a dielectric parameter that can be used to detect kissing bond.

Adhesive bonded specimens were tested for their dielectric properties. This included testing button specimens for their surface quality and single-lap joint specimens for their bond strength. Both bonded specimens were differently treated to simulate the kissing bond. Moreover, a relationship was worked out between the Dielectric Relaxation Strength and the shear strength of the single-lap joint specimens.

Thus, the comparison of the strength and quality of the bond by Dielectric Relaxation Strength confirmed that Broadband Dielectric Spectroscopy is a promising method to determine the bond nature. Moreover, this tool can be used to detect any exterior damage on the surface of the material or the adhesive bonded joint in airplanes.

Moreover, the hybrid composite specimens also prove that using BbDS, one can analyze the interfacial polarization occurring in a specimen, This, directly will give us an idea about the location where the charge gets accumulated, thus, ultimately leading us to the defective part of the specimen.

Chapter 9

FUTURE WORK

1. The samples of production materials supplied by our industrial partners need to be examined.
2. Construct an analysis of the results that'll help us to understand the physics and mechanics that is driving these correlations.
3. Find the limitations of the method.
4. Establish a more general experimental method for practical applications that may include thick materials, changes in temperature and moisture, and other industrial environments.
5. Develop an equation which will correlate the Dielectric Relaxation strength with the shear strength of the bonded specimen.

References

1. Brotherhood, C.J., Drinkwater, B.W., Dixon, S., “The detectability of kissing bonds in adhesive joints using ultrasonic techniques”, Elsevier Ultrasonics, Volume 41, Issue 7, September 2003, Pages 521-529
2. Hoke, M.J., “Adhesive Bonding of Composites”, Abaris Training Inc.
3. Baker, J., Adkins, J., Rabbi, F., Liu, Q., Reifsnider, K., Raihan, R., “Meso-design of heterogeneous dielectric material systems: Structure property relationships”, Journal of Advanced Dielectrics, Vol. 4, No. 2 (2014) 1450008 (9 pages)
4. Kremer, F., Dominguez, L., Meyer, W.H., Wenger, G., “Polymer”, 30:2023, 1989
5. Kremer, F., Schonhals, A., “Broadband Dielectric Spectroscopy”, Springer Verlag, 2002.
6. Davis, M.J., Bond, D.A., “The Importance of Failure Mode Identification in Adhesive Bonded Aircraft Structures and Repairs”, International Conference on Composite Materials, Vol. 12, 1999, Pages 5-9
7. Nagy, P.B. “Ultrasonic detection of kissing bonds at adhesive interfaces”, Adhesion Science Technology, 1991, Pages 619-630
8. Fazzino, P.D., Reifsnider, K.L., Majumdar, P., “Impedance spectroscopy for progressive damage analysis in woven composites”, Composites Science and Technology, 2009, Pages 2008-2014
9. Cawley, P., Pialucha, T., Lowe, M., “A Comparison of Different Methods for the Detection of a Weak Adhesive/Adherend Interface in Bonded Joints”, Review of Progress in Quantitative Nondestructive Evaluation, 1993, 1531-1538
10. Marty, P.N., “NDT of kissing bond in aeronautical structures”, 16th World Conference on NDT, 2004

11. Majumdar, P., Wilkes, C., Katiyar, P., Arnold, A., “Effect of Interfacial Defects on Mechanical Properties of Composite Materials Fatigue”, American Society of Composites, 2017
12. Psarras, G.C., Manolakaki, E., Tsangaris, G.M., “Dielectric dispersion and ac conductivity in-Iron particles loaded-polymer composites”, Composites Part A: Applied Science and Manufacturing, 2003, Pages 1187-1198
13. Psarras, G.C., Manolakaki, E., Tsangaris, G.M., “Electrical relaxations in polymeric particulate composites of epoxy resin and metal particles”, Composites Part A: Applied Science and Manufacturing, 2002, Pages 375-384
14. Raihan, R., (2014) “Dielectric Properties of Composite Materials during Damage Accumulation and Fracture”, Doctoral Thesis, University of South Carolina
15. Raihan, R., Cacuci, D., Liu, Q., Reifsnider, K., “Dielectric signatures and interpretive analysis for changes of statein composite materials”, Journal of Applied Mathematics and Mechanics, March 2015, Pages 1037-1045
16. Raihan, R., Adkins, J., Baker, J., Rabbi, F., Reifsnider, K., “Relationship of dielectric property change to composite material state degradation”, Composites Science and Technology, 2014, Pages 160-165
17. Täljsten, B. “The Importance of Bonding – An Historic Overview”, Proceedings of the International Symposium on Bond Behaviour of FRP in Structures, 2005
18. Vine, K.A., (1999) “The Non-destructive Testing of Adhesive Joints for Environmental Degradation”, Doctoral Thesis, University of London
19. Waugh, R.C. (2014) “Development of infrared techniques for practical defect identification in bonded joints” University of Southampton, Faculty of Engineering and the Environment, Doctoral Thesis, 209pp.

20. Judendorfer, T., Pirker, A., Muhr, M., “Conductivity measurements of electrical insulating oils”, IEEE International Conference on Dielectric Liquids, 2011
21. Elenchezhian, M., Vadlamudi, V., Banerjee, P.K., Dave, C., Mahmood, A., Raihan, R., Reifsnider, K., “Quality Assessment of Adhesive Bond based on Dielectric Properties” Society for the Advancement of Material and Process Engineering (SAMPE), Seattle 2017
22. Banerjee, P.K., Elenchezhian, M., Vadlamudi, V., Shute, N.,Raihan, R., Reifsnider, K., “Predicting Adhesive Bond Performance based on Initial Dielectric Properties”, American Society of Composites, 2017
23. Belingardi, G., Brunella, V., Martorana, B., Ciardiello, R., “Thermoplastic Adhesive for Automotive Applications”, Adhesives - Applications and Properties, Chapter 13, 2016
24. Broadband Dielectric/Impedance Spectrometers Documentation– Novocontrol Technologies – Brochures and Flyers.
25. Sabet, M., Soleimani, H., “Mechanical and electrical properties of low density polyethylene filled with carbon nanotubes”, 2nd International Conference on Structural Nano Composites, 2014
26. Swolfs, Y., Verpoest, I., Gorbatikh. L., “Tensile failure of hybrid composites: measuring, predicting and understanding”, 37th Risø International Symposium on Materials Science, 2016
27. Pandya, K.S., Veerraju. Ch., Naik, N.K., “Hybrid composites made of carbon and glass woven fabrics under quasi-static loading”, Materials & Design, Vol. 32, 2011, Pages 4094-4099

28. Swolfs, Y., Verpoest, I., Gorbatikh, L., “Maximising the hybrid effect in unidirectional hybrid composites”, Materials & Design, Vol. 93, 2016, Pages 39-45
29. Tuncer, E., Serdyuk, Y.V., Gubanski, S.M., “Dielectric mixtures – electrical properties and modeling”, arXiv preprint cond-mat/0111254

Biographical information

Priyanshu Kumar Banerjee, born on 13th January 1993, completed his Bachelor of Engineering in Mechanical Engineering from Yadavrao Tagaonkar College of Engineering and Management affiliated to the University of Mumbai, Maharashtra, India on May 2014.

He pursued his Masters in Mechanical Engineering from The University of Texas at Arlington starting January 2016. His master's thesis research work was under the supervision of Dr. Kenneth Reifsnider at the Institute for Predictive Performance Methodologies, a research wing of the University of Texas at Arlington Research Institute. His research interests include adhesive bonding in composites, computational modeling, polymer matrix composites, Broadband Dielectric Spectroscopy, destructive testing on materials and hybrid composites. During his master's degree at The University of Texas at Arlington, he also worked as a Research Assistant at the University of Texas at Arlington Research Institute in the Institute for Predictive Performance Methodologies.

He graduated with his master's degree from The University of Texas at Arlington in December 2017. He plans to continue his research on applying Broadband Dielectric Spectroscopy to adhesive bonding in composite materials and hybrid composites.